

# **Homeostatic scaling is driven by a translation-dependent degradation axis that recruits miRISC remodelling**

Balakumar Srinivasan<sup>1#</sup>, Sarbani Samaddar<sup>1#</sup>, Sivaram V.S. Mylavarapu<sup>2</sup>, James P. Clement<sup>3</sup> and Sourav Banerjee<sup>1§</sup>

1. National Brain Research Centre, NH-8. Nainwal Mode, Manesar-122052, Haryana, India

2. Regional Centre for Biotechnology, NCR-Biotech Science Cluster, Faridabad-Gurgaon Expressway, Faridabad-121001, Haryana, India

3. Neuroscience Unit, Jawaharlal Nehru Centre for Advanced Scientific Research, Jakkur, Bengaluru-560064, Karnataka, India.

# These authors contributed equally to this work

§ Correspondence

[souravnbrc@gmail.com](mailto:souravnbrc@gmail.com) OR [sourav@nbrc.ac.in](mailto:sourav@nbrc.ac.in) (S.B)

## 19 **Abstract**

20 Homeostatic scaling in neurons has been majorly attributed to the individual contribution of  
 21 either translation or degradation; however there remains limited insight towards understanding  
 22 how the interplay between the two processes effectuates synaptic homeostasis. Here, we  
 23 report that a co-dependence between the translation and degradation mechanisms drives  
 24 synaptic homeostasis whereas abrogation of either prevents it. Coordination between the two  
 25 processes is achieved through the formation of a tripartite complex between translation  
 26 regulators, the 26S proteasome and the miRNA-induced-silencing-complex (miRISC)  
 27 components such as MOV10 and Trim32 on actively translating transcripts or polysomes.  
 28 Disruption of polysomes abolishes this ternary interaction, suggesting that translating RNAs  
 29 facilitate the combinatorial action of the proteasome and the translational apparatus. We  
 30 identify that synaptic downscaling involves miRISC remodelling which entails the mTOR-  
 31 dependent translation of Trim32, an E3 ligase and the subsequent degradation of its target,  
 32 MOV10. MOV10 degradation is sufficient to invoke downscaling by enhancing Arc expression  
 33 and causing the subsequent removal of post-synaptic AMPA receptors. We propose a  
 34 mechanism that exploits a translation-driven degradation paradigm to invoke miRISC  
 35 remodelling and induce homeostatic scaling during chronic network activity.

## 36 **Introduction:**

37 Neurons employ a unique stratagem, known as synaptic scaling, to counter the run-away  
 38 excitation and subsequent loss of input specificity that arise due to Hebbian changes; they rely  
 39 on a compensatory remodelling of synapses throughout the network while maintaining  
 40 differences in their synaptic weightage (Burrone & Murthy, 2003; Keck *et al*, 2017; Turrigiano,  
 41 2017; Turrigiano & Nelson, 2004; Vitureira & Goda, 2013; Pozo & Goda, 2010). A complex

interplay of sensors and effectors within neurons serve to oppose global fluctuations in a network and establish synaptic homeostasis by modifying post-synaptic glutamatergic currents in a cell-autonomous manner (Davis, 2006; Ibata *et al*, 2008; Wierenga *et al*, 2006). In the context of homeostatic scaling, ‘sensors’ are classified as molecules that sense deviations in the overall network activity and ‘effectors’ scale the neuronal output commensurately.

Few molecular sensors of scaling have been identified to date; the eukaryotic elongation factor eEF2 and its dedicated kinase, eEF2 kinase or CamKIII are the two reported thus far (Sutton *et al*, 2007). However, there remains a huge chasm in identifying the repertoire of molecular cascades that serve to link events where neurons sense deviations in the network firing rate and subsequently initiate the scaling process. One such cascade is the mTORC1 (mammalian Target Of Rapamycin Complex-1) signalling pathway that regulates presynaptic compensation by promoting BDNF synthesis in the post-synaptic compartment (Henry *et al*, 2012, 2018). In contrast, AMPA-receptors (AMPA-Rs) have been identified, by overwhelming consensus, to be the predominant “end-point-effectors” in all paradigms of synaptic scaling (Gainey *et al*, 2009; O’Brien *et al*, 1998; Tataavarty *et al*, 2013; Thiagarajan *et al*, 2005). Unlike NMDARs, AMPARs undergo *de novo* translation during network destabilizations (Sutton *et al*, 2006) and chronic changes in the post-synaptic response during scaling has been attributed to the abundance of surface AMPARs (GluA1 and GluA2 subunits) (Lissin *et al*, 1998). Among the key modifiers of AMPAR expression, miRNAs are known to play pivotal roles in synaptic scaling (Hou *et al*, 2015; Letellier *et al*, 2014; Rajman *et al*, 2017; Silva *et al*, 2019). Relief from translational repression by miRNAs necessitates that mRNAs exit the functional miRISC, which entails that the latter undergo dynamic changes in its composition (Banerjee *et al*, 2009; Kenny *et al*,

2014). What remains surprising however, is our lack of knowledge about how compositional changes within the miRISC are achieved during the restoration of homeostasis.

The requirement for discrete sets of sensors and effectors is fulfilled within neurons through varied mechanisms including translation and ubiquitin-mediated proteasomal (UPS) degradation. An enhanced degradation of post-synaptic-density (PSD) proteins including GluA1 and GluA2 has been observed in contexts of altered network excitability (Ehlers, 2003) whereas complete inhibition of UPS activity was shown to occlude synaptic compensation (Jakawich *et al*, 2010). The integral role of *de novo* translation in sculpting the neuronal proteome was recently highlighted when proteomic analysis of neurons undergoing upscaling and downscaling revealed a remarkable diversity of newly synthesized proteins. Of particular interest was the significant enrichment in the expression of the proteasome core complex during the downscaling of synaptic activity (Schanzenbächer *et al*, 2016, 2018). The demand for the translation of proteasome complexes implies that proteasomes work alongside translation mechanisms during downscaling. Reports documenting the co-localization of ribosomes and the proteasome in neuronal dendrites (Bingol & Schuman, 2006; Ostroff *et al*, 2002) further emphasize the possibility that these two opposing machineries physically interact within the post-synaptic microcosm. The remodelling of the proteome through the dynamic regulation of protein biogenesis and degradation has been termed as cellular ‘proteostasis’ (Hanus & Schuman, 2013). However, several questions remain unexplored in the context of homeostatic scaling, such as a) what factor establishes the link between translation and protein degradation machineries to shape the proteome during scaling? b) Which process among translation and degradation takes precedence? c) What are the signalling mechanisms



86 that connect events of ‘sensing’ the bicuculline-mediated hyperactivity and the final down-  
87 regulation of AMPARs?

88 Here, we demonstrate a defined mechanism of synaptic scaling accomplished through the  
89 remodelling of miRISC *via* RNA-dependent coordination between translation and proteasome-  
90 mediated degradation. We observe that isolated inhibition of either translation or proteasomal  
91 activity offsets synaptic homeostasis and restoration of homeostasis necessitates the  
92 combination of both processes. We provide empirical evidence demonstrating that a direct  
93 interaction between translation and protein degradation machineries is achieved when the two  
94 apparatus are tethered to actively translating transcripts linked to miRISC. We find that in  
95 contexts of chronic hyperactivity, mTORC1-dependent translation of the E3 ligase Trim32  
96 promotes the degradation of MOV10, both members of the miRISC. Similar to hyperactivity-  
97 driven downscaling, the knockdown of MOV10 is sufficient to decrease the synaptic strength  
98 by reducing surface AMPARs. This occurs due to enhanced Arc expression following loss of  
99 MOV10. Comprehensively, our study shows that mTORC1 is triggered during synaptic  
100 downscaling to effectuate an RNA-dependent, translation-driven protein degradation axis that  
101 regulates miRISC remodelling to adjust the synaptic strength *via* Arc-mediated removal of  
102 surface AMPARs.

103

## 104 **Results**

### 105 **Co-dependence of protein synthesis and degradation drives synaptic homeostasis**

106 To test the existence of coordination between translation and degradation in the regulation of  
107 synaptic homeostasis, we measured miniature EPSCs (mEPSCs) from cultured hippocampal

neurons (DIV 18-24) after pharmacological inhibition of protein synthesis (anisomycin, 40 $\mu$ M) and proteasomal activity (lactacystin, 10 $\mu$ M) for 24 hours. Application of either lactacystin or anisomycin increased ( $2.99 \pm 1.23$  pA,  $p < 0.02$ ) and decreased ( $5.76 \pm 0.5$  pA,  $p < 0.01$ ) mEPSC amplitude respectively. Co-application of both inhibitors restored mEPSC amplitude to that of vehicle treated neurons (Figure 1A-B). The frequency of mEPSCs remained unaltered upon inhibition of translation and proteasome blockade either alone or in combination (Figure 1C), suggesting that this could be a post-synaptic phenomenon. Our data implies that interfering with either protein synthesis or degradation disturbs the balance of synaptic activity, while blocking both synthesis and degradation altogether restores it. Next, we stimulated synaptic downscaling using bicuculline (10 $\mu$ M, 24 hr) and observed that like previous reports, here too, chronic application of bicuculline lead to a significant decrease in mEPSC amplitude ( $5.56 \pm 0.31$  pA,  $p < 0.01$ ) without any detectable change in frequency (Figure 1D-F). The extent of decrease in mEPSC amplitude within bicuculline-treated neurons recapitulated the decrease observed in neurons where translation was blocked (bicuculline treated neuron  $5.56 \pm 0.31$  pA decrease vs. anisomycin treated neuron  $5.76 \pm 0.5$  pA decrease) (Figure 1B and 1E). We measured the mEPSC amplitude and frequency from hippocampal neurons when bicuculline was co-applied with anisomycin and lactacystin. The dual application of bicuculline and anisomycin did not result in any significant change in mEPSC amplitude when compared to neurons treated with bicuculline alone (Figure 1D-E). This confirms that, rather than inducing an additive effect,

Figure:1

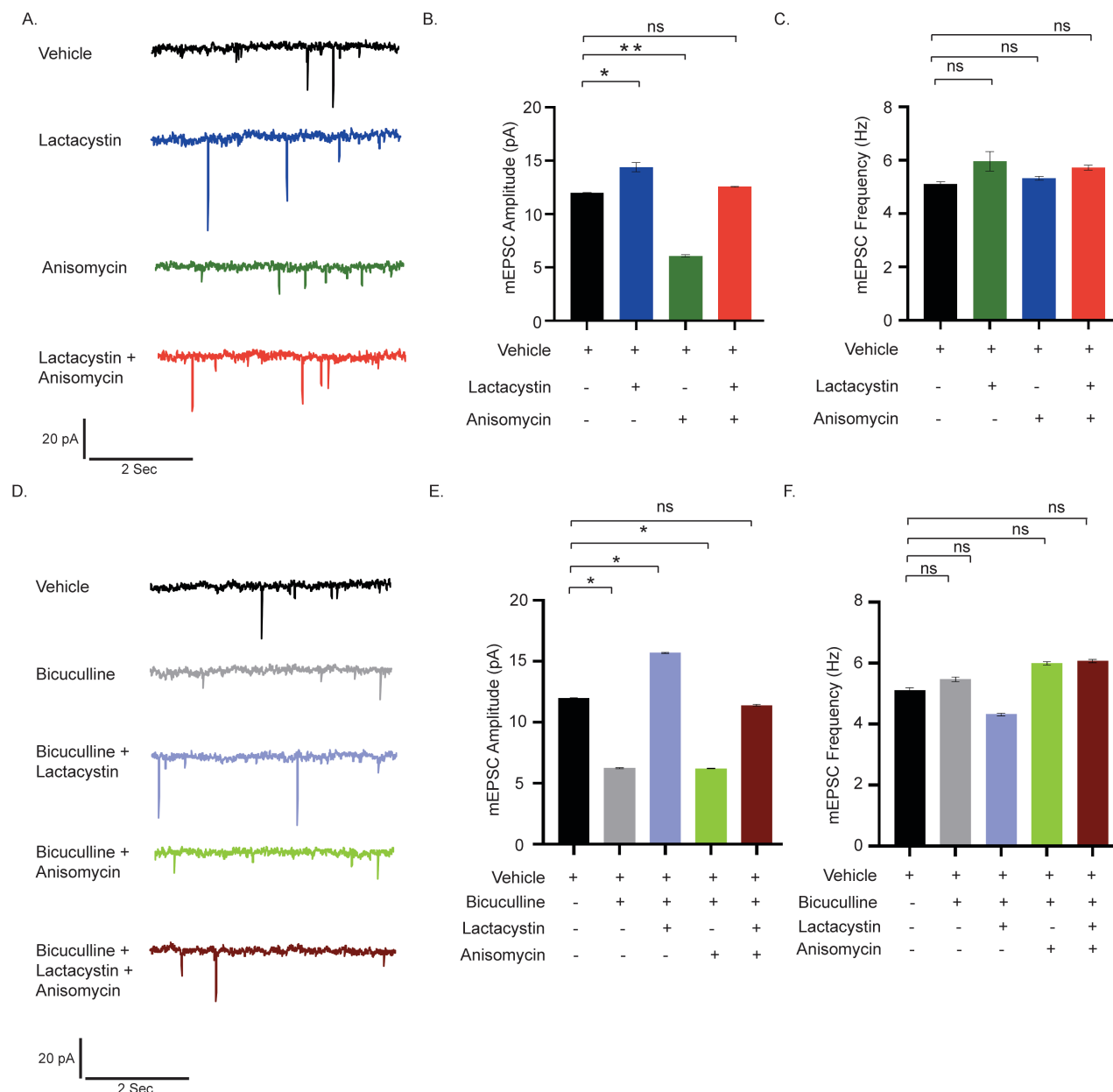


**Figure 1: Synaptic scaling is co-regulated by protein synthesis and degradation.**

(A-C) mEPSC traces from hippocampal neurons treated with vehicle, lactacystin, anisomycin and both (A). Mean mEPSC amplitude (B) and frequency (C).  $n=13-15$ . \* $p<0.024$ , \*\* $p<0.01$ . ns, not significant. Data shown as Mean  $\pm$  SEM. One Way ANOVA and Fisher's LSD. Scale as indicated.

(D-F) mEPSC traces from neurons treated with vehicle, bicuculline alone or in combination with lactacystin, anisomycin (D). Mean mEPSC amplitude (E) and frequency (F).  $n=12-16$ . \* $p<0.01$ . ns, not significant. Data shown as Mean  $\pm$  SEM. One Way ANOVA and Fisher's LSD. Scale as indicated.

chronic inhibition of protein synthesis in itself is sufficient to induce downscaling and could potentially override the effect observed due to bicuculline.

Disruption of proteasome function by lactacystin during bicuculline-treatment led to a significant increase in mEPSC amplitude ( $9.45 \pm 0.25$  pA increase as compared to bicuculline treated neurons,  $p < 0.01$ ) without altering frequency (Figure 1E-F). The increase was effectively more than the basal activity of vehicle-treated neurons ( $3.88 \pm 0.28$  pA,  $p < 0.01$ ) and mimicked the increase in mEPSC amplitude brought by lactacystin alone (Fig 1B and 1E). Although the influence of lactacystin on mEPSC amplitude is opposite to that of anisomycin, their individual effects override that of bicuculline in each condition. Co-application of both inhibitors during bicuculline-induced hyperactivation produced mEPSC amplitudes comparable to vehicle treated neurons (Figure 1E). Our data indicates that the co-inhibition of translation and degradation restricts any molecular changes away from the basal level, thus, maintaining the synaptic strength at the established physiological set point.

### **Synchronized translation and degradation regulates AMPAR distribution during scaling**

Since adjustment of synaptic strengths is directly correlated to the surface distribution of surface AMPARs (sAMPARs), we measured the surface expression of GluA1 and GluA2 (sGluA1/A2) to identify how concerted mechanisms of synthesis and degradation influence the distribution of sAMPARs during scaling. Neurons (DIV 21-24) were live-labelled using N-terminus specific antibodies against GluA1 and GluA2 following bicuculline treatment, either alone or in presence of both anisomycin and lactacystin for 24 hours and synapses marked by PSD95.

Figure: 2

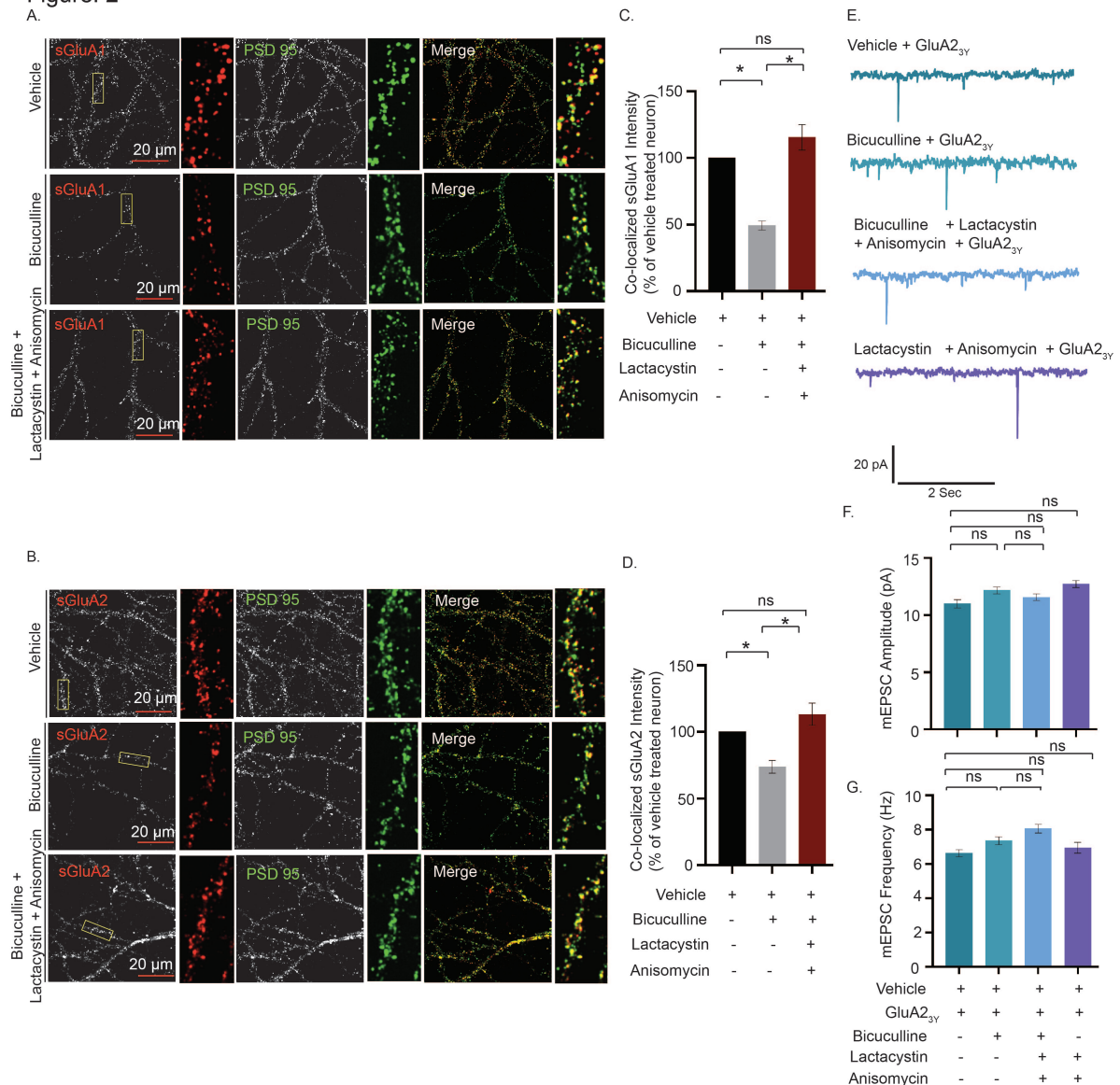


**Figure 2: Co-inhibition of protein synthesis and degradation restores hyperactivity driven reduction of synaptic AMPAR expression**

(A-D) High magnification images of sGluA1 or sGluA2 (red), PSD95 (green) and sGluA1/PSD95 (A) or sGluA2/PSD95 (B) (merged) images from neurons treated with vehicle, bicuculline alone or in combination with lactacystin and anisomycin. Normalized intensity of sGluA1 (C) or sGluA2 (D) co-localized with PSD95 particles. n=56-57, sGluA1 and n=31-63, sGluA2. \*p<0.01. Dendrite marked in yellow box was digitally amplified.

(E-G) mEPSCs traces from hippocampal neurons treated with GluA<sub>23y</sub> either alone or in presence of bicuculline, lactacystin + anisomycin and bicuculline + lactacystin + anisomycin (E). Mean mEPSC amplitude (F) and

frequency (G). n=10 - 13. ns, not significant. Data shown as Mean  $\pm$  SEM. One Way ANOVA and Fisher's LSD. Scale as indicated. See also Figure S1.

---

The surface expression of sGluA1/A2 in excitatory neurons was decreased following network hyperactivity ( $50.6 \pm 6.68\%$ ,  $p < 0.01$  for sGluA1 and  $26.1 \pm 6.62\%$ ,  $p < 0.01$  for sGluA2) (Figure 2A-D, S1 A-B). Consistent with our electrophysiological data, inhibition of both the translation apparatus and the proteasome in bicuculline-treated neurons increased sGluA1/A2 levels ( $133.95 \pm 8.77\%$ ,  $p < 0.01$  for sGluA1,  $53.17 \pm 6.44\%$ ,  $p < 0.0001$  for sGluA2) when compared to neurons treated with bicuculline alone (Figure 2C-D, S1A-B). Thus our data indicates that a dual inhibition of protein synthesis and degradation restores the synaptic sGluA1/A2 following network hyperactivity.

To reaffirm whether they are indeed the end-point effectors of synaptic downscaling, we used GluA2<sub>3Y</sub>, a synthetic peptide derived from the GluA2 carboxy tail of AMPA receptors to block the endocytosis of the AMPARs (Gainey *et al*, 2009), effectively ensuring the number of AMPARs to remain unchanged throughout 24 hours. Consistent with previous studies, no significant changes in mEPSC amplitude were detected upon inhibition of GluA2 endocytosis during chronic application of bicuculline (GluA2<sub>3Y</sub> treated neuron  $11.18 \pm 1.06$  pA vs. GluA2<sub>3Y</sub> + bicuculline treated neuron  $12.25 \pm 1.15$  pA,  $p < 0.49$ ) (Figure 2E-F). Application of GluA2<sub>3Y</sub> did not alter mEPSC amplitude as compared to vehicle treated neurons (GluA2<sub>3Y</sub> treated neuron  $11.18 \pm 1.06$  vs. vehicle treated neurons  $11.82 \pm 0.24$  pA) (Figure S1C-D), nor any change observed between neurons treated with GluA2<sub>3Y</sub> and those treated with both lactacystin and anisomycin in presence or absence of bicuculline (Figure 2F-G). mEPSC frequency remained unaltered throughout while mEPSC amplitude in each condition was

similar to that of control neurons (Figure 2G, S1E). Collectively, these observations indicate that changes in the abundance of surface-AMPA receptors during scaling is facilitated by proteomic remodelling that exploits both translation and degradation processes.

## **RNA-dependent tethering of the proteasome and translation regulators**

The co-localization of polyribosomes and proteasomes to sites of synaptic activity (Bingol and Schuman, 2006; Ostroff et al., 2002) indicate that the proteasomal machinery could remain physically associated with actively translating transcripts in order to make the necessary proteomic changes. To evaluate this, we analysed polysomes from the hippocampus of 8-10 week old rat and assessed whether the sedimentation pattern of proteasomes matches those of actively translating, polyribosome-associated mRNA fractions. We observed that several components of the proteasomal machinery such as  $\alpha 7$  subunit of 20S; Rpt1, Rpt3 and Rpt6 subunits of the 19S proteasome co-sedimented with translation initiation factors such as eIF4E, p70S6 kinase and its phosphorylated form, the regulatory kinase of mTORC1-mediated protein synthesis within actively translating polysomes (Figure 3A-B, S2A). We also detected the polysomal distribution of MOV10, an RNA binding protein known to be poly-ubiquitinated upon synaptic activation, and Trim32, an E3 ligase, both components of the miRISC (Schwamborn et al, 2009) (Figure 3A-B).



Figure:3

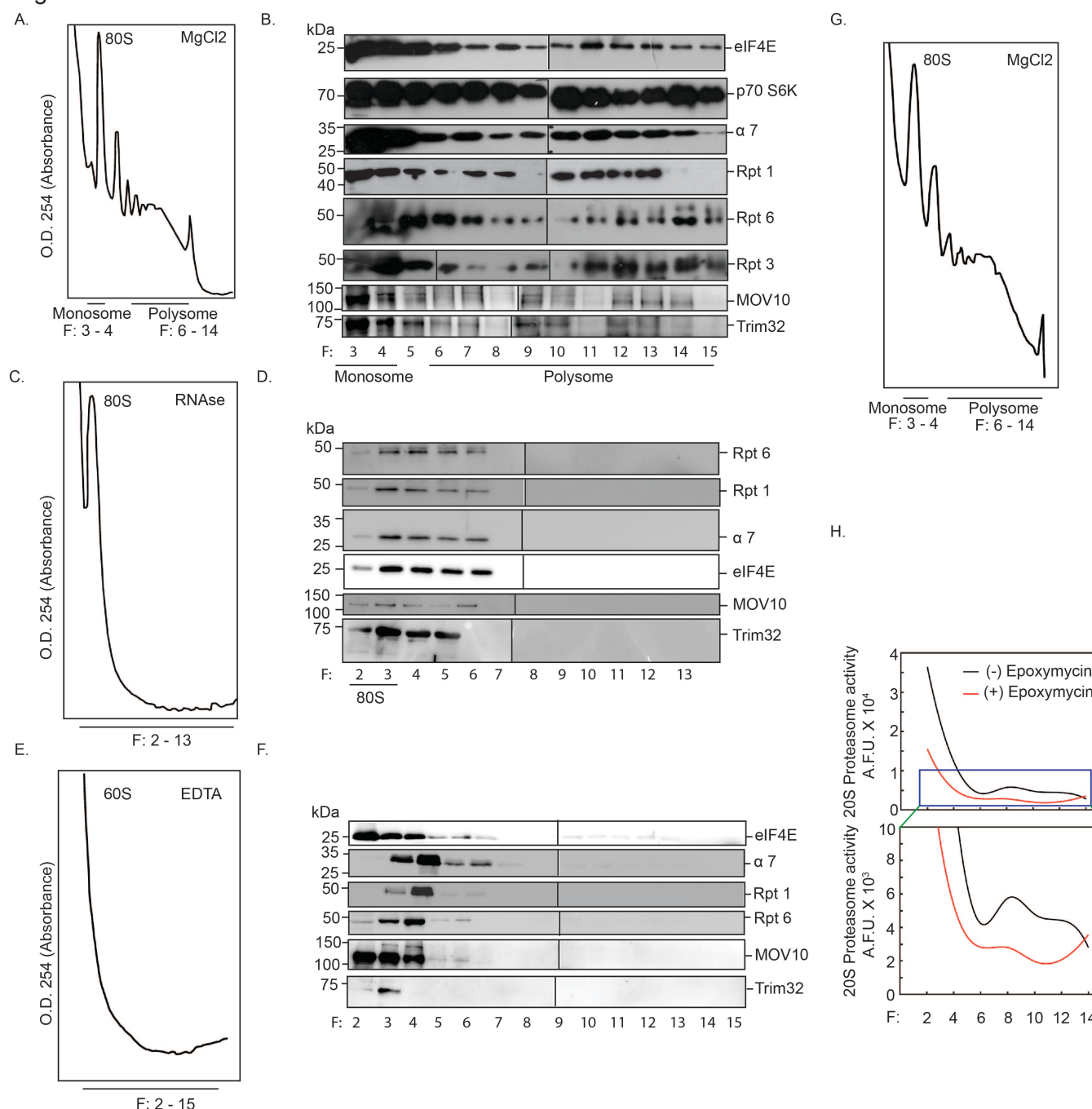


**Figure 3: RNA-dependent association between active proteasomes and translating polyribosomes**

(A-F) Absorbance profile at 254nm ( $A_{254}$ ) of fractionated cytoplasmic extracts from hippocampal tissue incubated without (A) or with RNase (C) or with EDTA (E). Monosome (80S) or 60S Ribosome or Polysome fractions as indicated. Western blot analysis of fractions without (B) or with RNase (D) or with EDTA (F) treatment showing



distribution of translation regulators eIF4E and p70S6 Kinase;  $\alpha$ 7 subunit of 20S core and Rpt1, Rpt3, Rpt6 of 19S cap; miRISC proteins MOV10 and Trim32.

(G-H)  $A_{254}$  profile of fractionated cytoplasmic extract (G) and quantitation of catalytic activity of proteasomes present in alternate fractions from two polysome preparations (H). See also Figure S2.

---

RNAse or EDTA treatment of cytoplasmic lysates prior to density gradient fractionation led to a complete collapse of the polysome profile, simultaneously shifting the sedimentation of the proteasome subunits, E3 ligase, translation regulators and RNA binding proteins to the lighter fractions (Figure 3C-F, S2B-C). The disruption of association between the translational and proteasomal modules on RNAse and EDTA treatment suggests that translating transcripts act as scaffolds to facilitate their tripartite interaction. These observations ruled out a possible causality for the observed co-sedimentation due to similar densities of protein complexes associated with translation and proteasome machineries. Furthermore, we observed that the polysome-associated 26S proteasome is catalytically active as detected by its ability to cleave a fluorogenic proteasome substrate that is blocked by proteasome inhibitor epoxymycin (Figure 3G-H, S2D).

**Proteasome and the regulators of translation directly interact with each other within excitatory neurons.**

Whole-cell patch clamp recordings demonstrating that the co-regulation of translation and proteasome-mediated protein degradation is necessary for synaptic homeostasis, was measured from excitatory hippocampal neurons.

Figure: 4

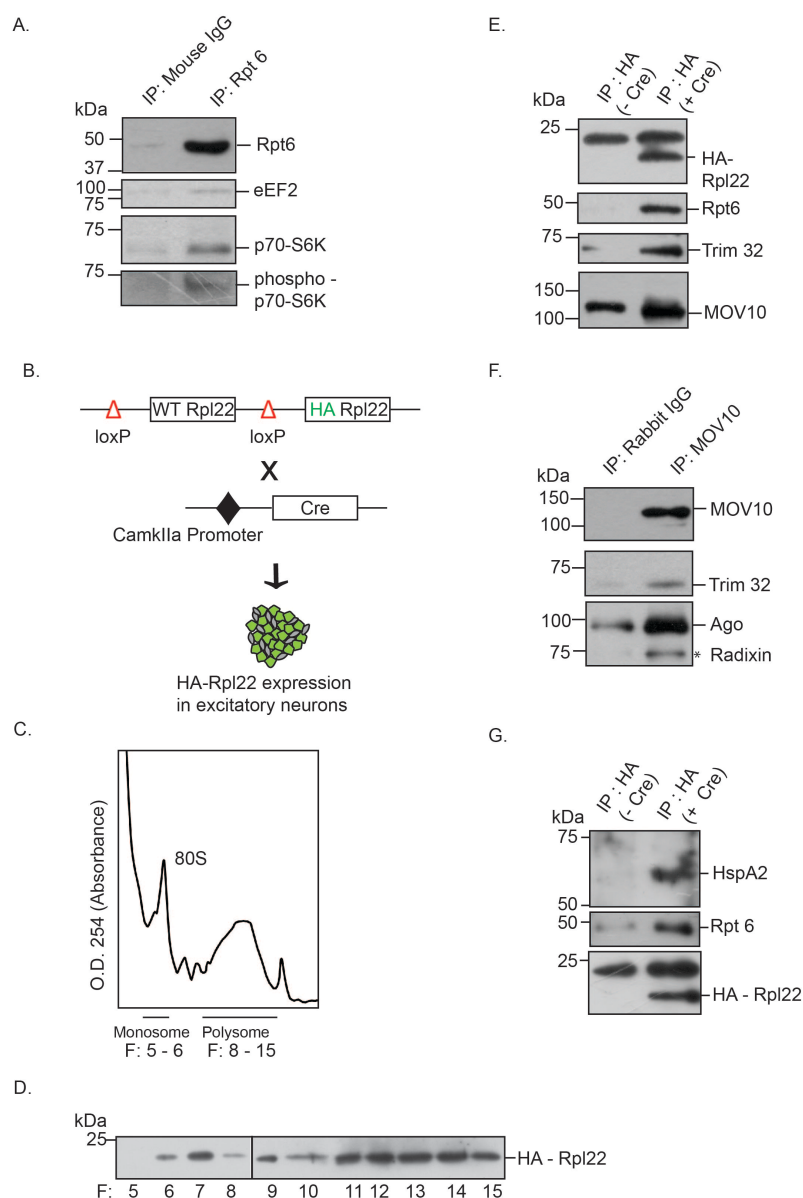


**Figure 4: Interaction between proteasome and actively translating RNA-associated polyribosomes.**

(A) Proteasome associated protein complex was immunoprecipitated from hippocampal lysate using antibody against Rpt6 and mouse IgG. Western blot of purified protein complex using antibodies against eEF2, p70S6 Kinase, phospho-p70S6 kinase. (B) RiboTag mouse crossed with CamkIIa promoter- driven Cre recombinase mouse results in deletion of wild-type Rpl22 ribosomal protein and replacement of HA tagged Rpl22 in forebrain excitatory neurons. (C)  $A_{254}$  profile showing indicated fractions of Monosome and Polysome. (D) Polysome fractions showing enrichment of HA-Rpl22 as detected by western blot using antibody against HA. (E) HA-

tagged Rpl22 containing polyribosome affinity purified using antibody against HA. Western blot analysis of affinity purified complex using antibodies against HA, Rpt6, Trim32 and MOV10. (F) MOV10 was immunoprecipitated from hippocampal lysate. Western blot analysis of MOV10-immunoprecipitated protein complex showed the co-precipitation of Trim32 with miRISC components MOV10 and Ago. (G) Detection of HspA2 and Rpt6 in HA affinity purified protein complex from HA-Rpl22 expressing neurons by western blot using antibody against HspA2 and Rpt6 and HA.

---

Consistent with this observation, co-sedimentation of proteasome subunits along with translating mRNA linked to protein synthesis regulators including miRISC led us to enquire whether components of ternary complex directly interact with each other in excitatory neurons of hippocampus. To evaluate this, we immunoprecipitated the 19S proteasomal complex using Rpt6 antibody from hippocampal neurons. We observed the co-precipitation of eEF2, a translation elongation factor that functions as a “sensor” of change in network activity (Figure 4A). We also found that p70S6 kinase as well as its phosphorylated form- a known regulator of the mTORC1-dependent protein synthesis (Ma & Blenis, 2009) co-precipitated with the 19S proteasome (Figure 4A). We further analyzed the proteins interacting with polysomes within excitatory neurons by expressing Hemagglutinin (HA) tagged ribosomal protein Rpl22 (HA-Rpl22) that gets incorporated into polysomes (Sanz *et al*, 2009; Shigeoka *et al*, 2016) (Figure 4B-D, S2E). We reasoned that the analysis of HA-Rpl22-affinity purified complexes would confirm whether the polysome-associated translation and degradation machineries directly interact with each other. Our western blot analysis of HA-Rpl22 affinity-purified protein complex showed that Rpt6 directly interacts with Trim32 and MOV10 (Figure 4E). The interaction of MOV10 with ribosomes is crucial as it gives credence to the association of miRNAs with polysomes, as per previous reports (Krichevsky *et al*, 2003). Immunoprecipitation of MOV10 from hippocampal neurons allowed us to detect the co-precipitation of both Argonaute (Ago)

and Trim32, confirming that the latter is an integral component of the Ago-containing miRISC (Figure 4F). We also detected the chaperone protein HspA2 in the HA-affinity purified fraction along with Rpt6 (Figure 4G), suggesting that HspA2 could tether proteasomes to actively translating transcripts.

## **Protein synthesis drives mTORC1-dependent proteasomal degradation to cause miRISC remodelling during synaptic downscaling**

Association between MOV10 and Trim32, all members of the miRISC, and their direct interaction with protein synthesis as well as degradation machineries led us to analyze whether concerted translation and degradation during bicuculline induced chronic network hyperactivity could influence miRISC remodelling. Bicuculline treatment of hippocampal neurons (DIV 18 - 21) enhanced ( $101.7 \pm 10.06\%$  increase,  $p < 0.0001$ ) Trim32 with a concomitant decrease ( $65.94 \pm 2.67\%$  decrease,  $p < 0.001$ ) in MOV10 (Figure 5A-C). The increase in Trim32 expression post bicuculline treatment was blocked by anisomycin and surprisingly resulted in the inhibition of MOV10 degradation ( $82.28 \pm 12.90\%$  protected MOV10,  $p < 0.03$ ) (Figure 5C). This indicates that the degradation of MOV10 is dependent on enhanced Trim32 synthesis and that Trim32 translation precedes the commencement of MOV10 degradation. Treatment with lactacystin resulted in the expected protection of MOV10 from degradation ( $71.93 \pm 5.74\%$  MOV10 protected,  $p < 0.01$ ) upon bicuculline-induced hyperactivity (Figure 5C); whereas there remained no change in the Trim32 expression levels (Figure 5B). Moreover, co-application of lactacystin and anisomycin during bicuculline-induced hyperactivity changed the expression of MOV10 and Trim32 commensurate to basal levels (Figure 5B-C). We have also analyzed Trim32 and MOV10 expression after anisomycin and lactacystin treatment, either alone or in

combination, to assess the necessity of chronic hyperactivity in the co-ordinated control of miRISC remodelling. We observed that the chronic inhibition of protein synthesis led to a modest but statistically significant decrease of both Trim32 ( $22.42 \pm 0.70\%$  decrease,  $p < 0.001$ ) and MOV10 ( $28.14 \pm 0.48\%$  decrease,  $p < 0.0003$ ) (Figure S3A-C). However, chronic inhibition of proteasome has no effect on Trim32 and MOV10 expression (Figure S3A-C). We reasoned that the significant decrease of both proteins was observed due to combined effect of global inhibition of translation and ongoing basal level of protein degradation. These observations indicate that the miRISC remodelling occurs in conditions of chronic network hyperactivity induced by bicuculline.

Reciprocal patterns between MOV10 and Trim32 expression levels led us to analyse whether the latter is the E3-ligase responsible for the UPS-mediated degradation of MOV10. Consistent with our hypothesis, knockdown of Trim32 ( $85.43 \pm 4.04\%$  knockdown,  $p < 0.01$ ) by shRNA-mediated RNAi enhanced the expression of MOV10 ( $44.74 \pm 14.33\%$  increase,  $p < 0.02$ ) (Figure 5D-F), suggesting that Trim32 translation drives the proteasome-mediated degradation of MOV10 and that it may be sufficient for MOV10 ubiquitination and subsequent degradation. These observations show that Trim32 translation drives the proteasome-mediated degradation of MOV10 and suggests that Trim32 may be the only miRISC-associated E3 ligase required for MOV10 ubiquitination.

Figure: 5

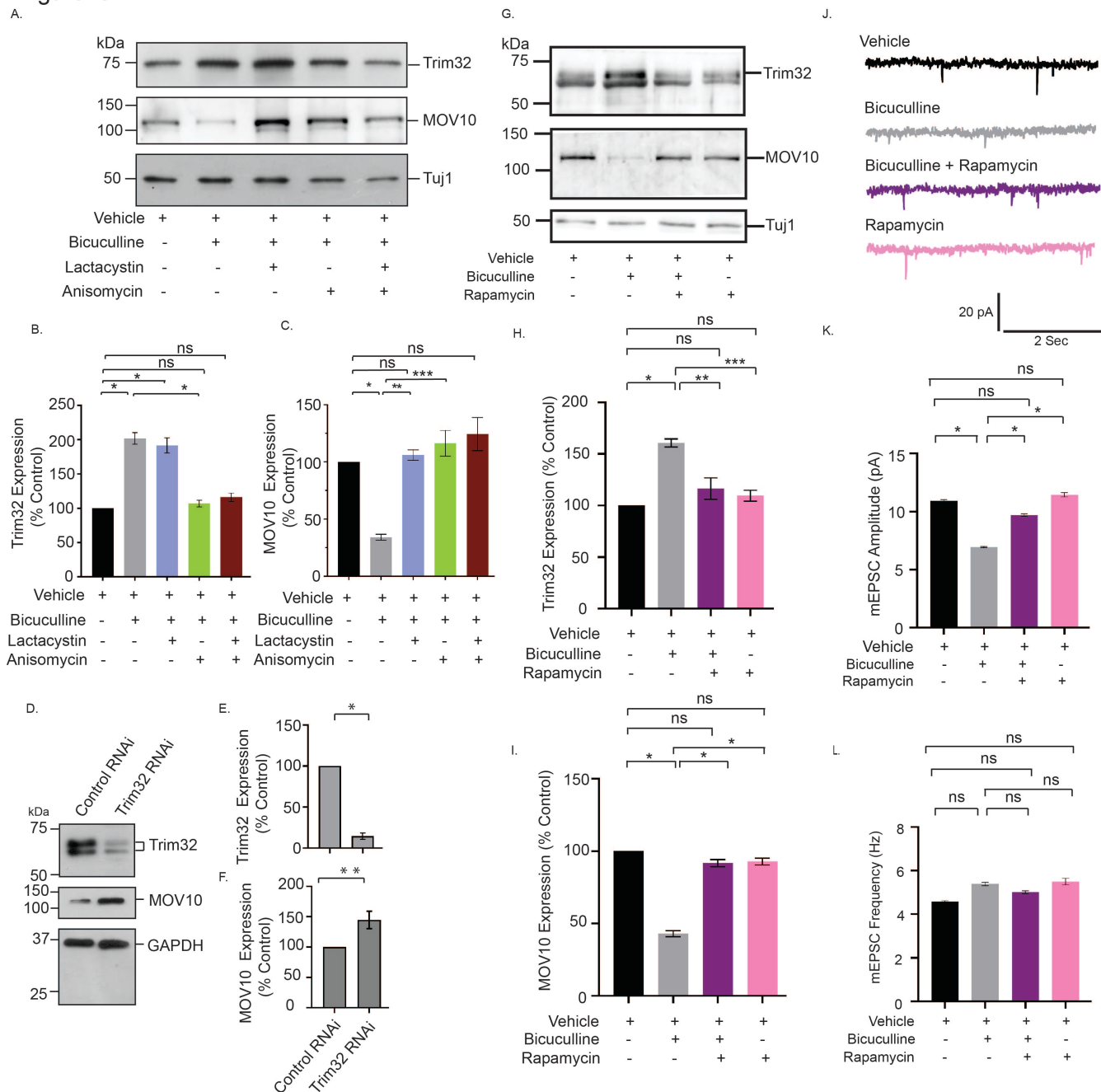


**Figure 5: Synthesis of Trim32 facilitates MOV10 degradation and requires activation of mTORC1**

(A-C) Western blot analysis showing the expression of Trim32, MOV10 and Tuj1 from neurons treated with bicuculline with or without lactacystin, anisomycin or both (A). Quantitation of Trim32 (B) and MOV10 (C) expression.  $n=3$ . Data shown as Mean  $\pm$  SEM. \* $p<0.0001$  (B) and \* $p<0.001$ , \*\* $p<0.006$ , \*\*\* $p<0.02$  (C). ns, not significant. One Way ANOVA and Fisher's LSD.

(D-F) Western blot analysis of neurons infected with lentivirus expressing Trim32 or non-targetting control shRNA showing expression of Trim32, MOV10 and Tuj1 (D). Quantitation of Trim32 (E) and MOV10 (F). n=5. Data shown as Mean  $\pm$  SEM. \*p<0.01, \*\*p<0.02. Unpaired t-test with Welch's correction.

(G-I) Western blot analysis from neurons treated with bicuculline, Rapamycin or both. showing expression levels of Trim32, MOV10 and Tuj1 (G). Quantitation of Trim32 (H) MOV10 (I) expression. Data shown as Mean  $\pm$  SEM. n=5. \*p<0.0001, \*\*p<0.0007, \*\*\*p<0.0001 (H) and \*p<0.001 (I). ns, not significant. One Way ANOVA and Bonferroni's correction. See also Figure S2.

(J-L) mEPSC traces from neurons treated with vehicle, bicuculline, rapamycin or both (J). Mean mEPSC amplitude (K) and frequency (L). n=8-9. \*p<0.01. ns, not significant. Data shown as Mean  $\pm$  SEM. One Way ANOVA and Fisher's LSD.

---

Having observed the co-precipitation of the downstream effectors of the mTORC1 signalling cascade with the 26S proteosomal subunit Rpt6, we focused on identifying whether mTORC1 signalling plays a role in causing synaptic downscaling in response to chronic hyperactivity. Bicuculline-treatment of hippocampal neurons in the presence of rapamycin (100nM, 24 hr), a selective inhibitor of mTORC1, completely abolished chronic hyperactivity-driven Trim32 synthesis ( $16.48 \pm 8.6\%$  increase as compared to control, p=0.99) and consecutive MOV10 degradation ( $8.19 \pm 2.81\%$  decrease as compared to control, p=0.06) (Figure 5G-I). Rapamycin treatment alone did not alter the expression patterns of Trim32 and MOV10 (Figure 5G-I). This led us to hypothesize that mTORC1 pathway acts upstream of Trim32, serving to regulate its synthesis in response to bicuculline. Chronic bicuculline treatment lead to a significant enhancement of p70S6 kinase phosphorylation ( $92.07 \pm 20.22\%$  increase, p<0.001) which was blocked by rapamycin (Figure S3D-E), indicating that the mTORC1 signalling cascade is key in effectuating bicuculline-induced synaptic downscaling. Consistent with our biochemical data, we observed that co-incubation of rapamycin and bicuculline prevented the decrease in mEPSC amplitude ( $2.47 \pm 0.26$  pA increase as compared to



bicuculline treated neurons,  $p < 0.01$ ) but not frequency (Figure 5J-L). Just as above, rapamycin treatment alone has no effect, indicating that chronic hyperactivity acts as a triggering point for mTORC1 activation (Figure 5K-L) and this subsequently plays a role in driving TRIM32 translation.

### **MOV10 degradation is sufficient to invoke downscaling of AMPARs**

MOV10 is an integral component of miRISC and its removal from the protein complex disrupts miRISC function. MOV10 degradation in response to chronic bicuculline treatment, made us question whether its loss alone was sufficient to cause pervasive changes in the miRISC and bring about synaptic downscaling. We mimicked hyperactivity-driven MOV10 degradation by lentivirus-mediated RNAi of MOV10. Intensity of sGluA1/A2 puncta that co-localized with PSD95 was analyzed following MOV10 knockdown (DIV21-24). We observed that loss of MOV10 reduced the expression of sGluA1 ( $35.03 \pm 9.35$  % for shRNA#1,  $p < 0.01$  and  $58.38 \pm 10.27$  % for shRNA#2,  $p < 0.01$ ) and sGluA2 ( $49.4 \pm 12.9$  % for shRNA#1,  $p < 0.01$ ) at the synapses (Figure 6A-D, S4), that recapitulated the re-distribution of sGluA1/sGluA2 in neurons under chronic bicuculline treatment (Figure 2C-D). The knockdown of MOV10 reduced mEPSC amplitude ( $3.48 \pm 0.24$  pA for shRNA#1 and  $4.05 \pm 0.23$  pA for shRNA#2,  $p < 0.01$ ) but not frequency (Figure 6E-G), an observation that mirrors synaptic downscaling following bicuculline treatment (Figure 1E). We have used two shRNAs against MOV10 for its effective knockdown and also a non-targeting shRNA to eliminate the possibility of an off-target effect.



Figure: 6

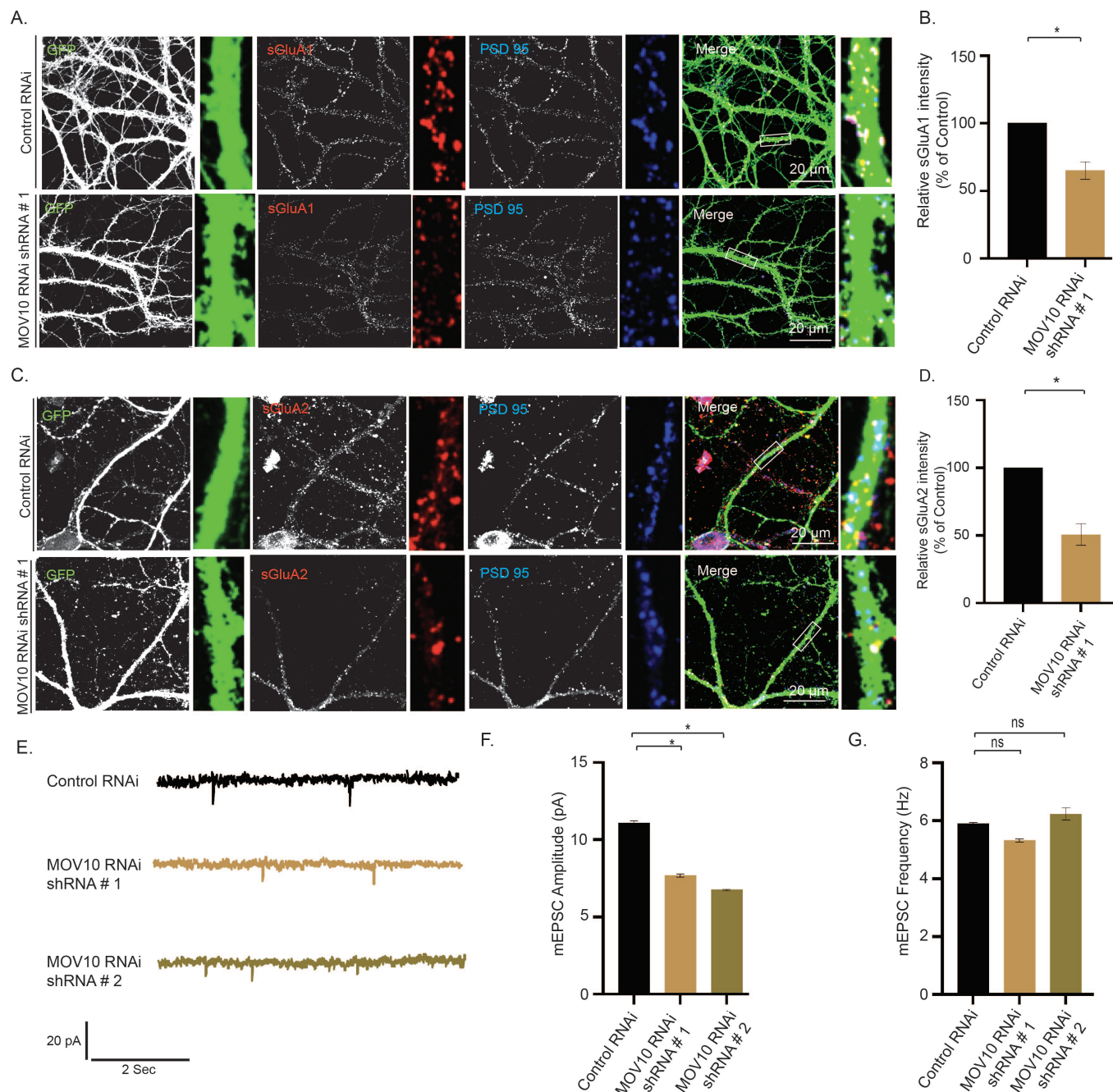


**Figure 6: MOV10 regulates synaptic activity by modulating abundance of sAMPA**

(A-D) High magnification images of neurons transduced with lentivirus co-expressing EGFP and MOV10 or non-targeting shRNA showing expression of sGluA1 (A) or sGluA2 (C) (red), PSD95 (blue), GFP (green) and GFP/sGluA1/PSD95 or GFP/sGluA2/PSD95 (merged). Quantitation of normalized intensity of synaptic sGluA1 (B)

or sGluA2 (D). n=26 - 30, GluA1; n=12 – 15, GluA2. Data shown as Mean  $\pm$  SEM. \*p<0.01. One Way ANOVA and Fisher's LSD. Dendrite marked in yellow box was digitally amplified. See also Figure S3.

(E-G) mEPSC traces from transduced neurons (E). Mean mEPSC amplitude (F) and frequency (G). n=12 – 13. \*p<0.01. ns, not significant. Data shown as Mean  $\pm$  SEM. One Way ANOVA.

---

How MOV10 degradation leads to the removal of sAMPA receptors to regulate synaptic downscaling? Arc/Arg3.1, an immediate early gene, has been shown to be dynamically regulated by chronic changes in synaptic activity, and evokes synaptic scaling (Shepherd *et al*, 2006). Overexpression of Arc decreases sAMPA receptors *via* endocytosis whereas its knockdown increases them (Chowdhury *et al*, 2006). Arc expression has been shown to be regulated by diverse mechanisms including translational control that involves miRNAs (Wibbrand *et al*, 2012; Paolantoni *et al*, 2018). These observation prompted us to analyze the Arc expression following MOV10 knockdown. We observed that the loss of MOV10 enhanced Arc ( $106.4 \pm 11.92\%$  increase, p<0.003 for shRNA # 1 and  $176.1 \pm 20.24\%$  increase, p<0.003 for shRNA # 2) (Figure 7A-B). The extent of increase in Arc protein was commensurate with the efficacy of two shRNAs against MOV10 (Figure 7A-B). We also observed that this differential enhancement of Arc is reflected in the proportionate removal of sAMPA receptors and concomitant decrease in mEPSC amplitude (Figure 6E). Our data showed that bicuculline-induced chronic hyperactivity, which degrades MOV10, also enhanced Arc expression ( $132.1 \pm 27.45\%$  increase, p<0.04) (Figure 7C-D). This activity-driven enhancement of Arc is blocked by the inhibition of mTORC1 by rapamycin (100nM, 24 hr). We observed that rapamycin treatment alone has no effect (Figure 7C-D).

**Figure 7**

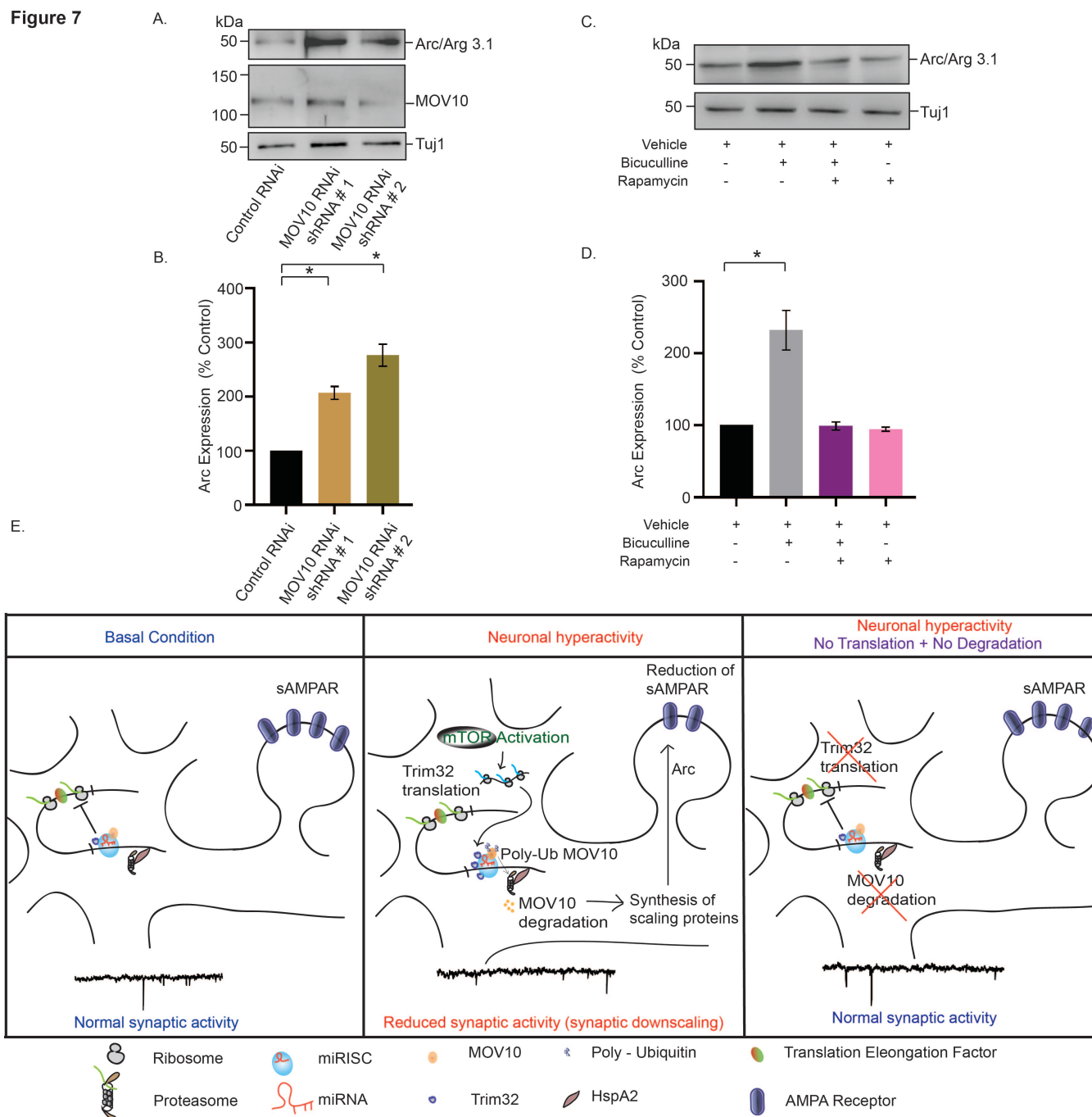


**Figure 7: mTORC1-mediated regulation of Arc expression upon chronic hyperactivity involves MOV10**

(A-B) Western blot analysis showing the Arc protein level after MOV10 knockdown in neurons infected with lentivirus expressing two different shRNAs against MOV10 (A). Quantitation of Arc expression (B). n=4.\* p<0.003. Data shown as Mean  $\pm$  SEM. One Way ANOVA and Fisher's LSD.

(C-D) Western blot analysis of neurons treated with bicuculline in presence or absence of rapamycin showing the expression of Arc protein (C). Quantitation of Arc expression (D). n=3. \*p<0.04. Data shown as Mean ± SEM. One Way ANOVA and Fisher's LSD.

(E) Schematic representation showing maintenance of homeostatic synaptic activity by coordinated control of protein synthesis and degradation that modulates composition of miRISC.

---

Taken together, our data demonstrates that the bicuculline-induced downscaling of synaptic strength occurs *via* an mTORC1-mediated translation-dependent proteasomal degradation of MOV10 involving removal sAMPA receptors *via* Arc (Figure 7E).

## Discussion

Here we provide empirical evidence emphasizing that synchrony between protein synthesis and proteasomal activity is critical to establish homeostasis at synapses. We used a paradigm of chronic network hyperactivity to invoke downscaling and determined a) translation and degradation apparatuses remain linked by RNA scaffolds; b) it is the translation of Trim32 that drives the degradation of MOV10 to cause miRISC remodelling, thus the current paradigm is an example of translation preceding degradation; c) miRISC is a key node in the translation-degradation axis, with mTORC1 being the upstream signalling component which is a part of the 'sensor' machinery, and Arc-induced removal of sAMPA receptors being the final effectors of downscaling.

## Co-regulation of protein synthesis and degradation drives AMPAR-mediated synaptic downscaling

We find that chronic perturbation of either translation or proteasomal activity occludes synaptic homeostasis, while homeostasis remains unperturbed when there is simultaneous inhibition of

both. Chronic application of bicuculline along with either lactacystin or anisomycin leads to alterations of mEPSC amplitude that exactly mirror observations where bicuculline is absent (Figure 1B vs Figure 1E). Thus, the effects of bicuculline-induced changes to the existing proteome are overshadowed by those accomplished by the individual action of the proteasome or the translation machinery (Figures 1). mEPSC frequency remain unaltered in all conditions. The importance of these observations is multi-faceted; it establishes that, i) congruent protein synthesis and degradation pathways regulate synaptic scaling; ii) the constancy of the proteomic pool in the presence of lactacystin and anisomycin renders the effect of any network destabilizing stimuli like bicuculline to be redundant, and iii) long-term changes in the proteome predominantly affects the physiology of the post-synaptic compartment.

Our observations echo previous findings in Hebbian plasticity; wherein, protein synthesis during LTP/LTD was required to counter the changes in the proteomic pool triggered by protein degradation. The blockade of L-LTP accomplished by inhibiting protein synthesis was revoked on the simultaneous application of proteasomal blockers and translational inhibitors (Fonseca *et al*, 2006). Abrogation of proteasomal activity allowed mGluR-dependent LTD to proceed even in the absence of protein synthesis (Klein *et al*, 2015). These observations emphatically suggest the existence of a proteostasis network that enable compositional changes to the proteome in contexts of acute or chronic changes in synaptic function (Jayaraj *et al*, 2020; Cajigas *et al*, 2010; Hanus & Schuman, 2013). As LTP and LTD modify the cellular proteome through the simultaneous recruitment of protein synthesis and degradation; it stands to reason that homeostatic scaling mechanisms may also employ a functional synergy of the two to recompense for the changes brought about by unconstrained Hebbian processes.

AMPA-mediated currents decrease more than NMDAR currents during chronic network hyperactivity (O'Brien *et al*, 1998; Lissin *et al*, 1998) and unlike NMDARs, the turnover of AMPARs is translation-dependent (Goold & Nicoll, 2010). The surface distribution of AMPARs, therefore remain accurate readouts of synaptic output. We wanted to confirm whether the combined action of translation and degradation affect post-synaptic scaling through any other effectors and reasoned that if synaptic strength is dominated by changes in AMPAR currents, restricting changes to the sAMPA abundance should prevent the scaling of mEPSCs even under chronic hyperactivity. Similar to the observations in synaptic upscaling (Gainey *et al*, 2009), the inhibition of GluA2-endocytosis by GluA2<sub>3Y</sub> peptide also blocked synaptic down scaling (Figure 2); reinforcing that AMPARs indeed remain the end-point effectors despite changes to the proteome.

## **RNA-dependent association of the translation and degradation apparatus underlie their functional coherence**

The co-localization of polyribosomes and proteasomes in neuronal subcompartments suggest that for translation and proteasomal degradation to work in tandem, physical proximity between the two modules cannot be ruled out (Bingol & Schuman, 2006; Ostroff *et al*, 2002). Polysome analysis showed the co-sedimentation of members of the 19S proteasome (Rpt1, Rpt3 and Rpt6 subunits) and the 20S proteasome ( $\alpha$ 7 subunit) along with translation initiation factors such as eIF4E and p70S6 kinase, a downstream effector of mTORC1. Abrogation of the sedimentation pattern in the presence of RNase and EDTA, is indicative of an RNA-dependent direct interaction between translation and protein degradation (Figure 3). Affinity purification of polyribosomes containing HA-Rpl22 confirmed that there is direct interaction between



members of the two modules (Figure 4). Such existence of direct interaction between polyribosome and catalytically active proteasomes allows close temporal coordination between translation and protein degradation. How do protein degradation machineries remain tethered to actively translating mRNAs? We have identified that HspA2 (Hsp70 family), a chaperone protein, remains tethered to proteasomes (Figure 4). Hsp70 family of proteins is known to influence both the synthesis and degradation of proteins by their association with 26S proteasomal subunits (Tai *et al*, 2010) and translation initiation factors (Shalgi *et al*, 2013). HspA2 therefore, is a component of proteostasis coordinators which includes proteasome, translation regulators and chaperon proteins.

#### **mTORC1-mediated Trim32 synthesis precedes MOV10 degradation during downscaling**

The co-incident detection of MOV10 and miRNAs from polysome fractions purified from neurons give credence to the existence of a tripartite (translating RNA associated miRISC – proteasome complex – translation apparatus) regulatory axis underlying scaling. Under the chronic influence of bicuculline, synthesis of the E3 ligase Trim32 precedes the degradation of MOV10, the alternative possibility that MOV10 degradation leads to increased *de novo* translation of Trim32, is not supported, since protein synthesis inhibition by anisomycin leads to MOV10 rescue (Figure 5). Loss of the E3-ligase Trim32 elevated the basal level of MOV10, indicating a ubiquitin-dependent degradation by the proteasome (Figure 5). Although MOV10 has been shown to also regulate miRISC-independent function to modulate RNA modification (Warkocki *et al*, 2018) and stability (Gregersen *et al*, 2014), association of MOV10 with Argonaute indeed emphasize the remodelling of miRISC during synaptic downscaling. What post-synaptic signalling cascade triggers Trim32 translation? We find that chronic bicuculline

induction triggers the mTORC1-dependent synthesis of Trim32 that is abrogated on rapamycin treatment (Figure 5). Identification of the mTOR downstream effector p70S6 kinase within the tripartite complex further suggests that the mTOR signalling is crucial for driving proteostasis.

A recent study has demonstrated that a slow turnover of plasticity proteins (measured at 1,3 and 7 days in cultured neurons) is essential to create long-term changes to the neuronal proteome during both up and down-scaling (Dörrbaum *et al*, 2020). The authors have argued that the slow turnover rate is more energy-saving and therefore a preferred cellular mechanism. However, this study also identifies a very small fraction of previously reported scaling factors with fast turnover rates specifically influencing up- and down- scaling. Our reports support the latter findings, where we observe that both the increase in Trim32 synthesis and the resulted degradation of MOV10 happen within 24 hours during synaptic downscaling, suggesting a fast turnover. As both MOV10 and Trim32 are part of the miRISC, their fast turnover rates seems plausible, considering that participation of the miRISC to relieve the translational depression of several transcripts encoding plasticity proteins needs to happen fast in order to boost changes to the proteome. Although in terms of energy expenditure the coordinated regulation of translation and degradation is expensive, this cellular trade-off may be necessary to trigger the remodelling of a very limited number of master regulators of the neuronal proteome, such as miRISC, during synaptic downscaling.

### **Degradative control of miRISC remodelling underlies homeostatic scaling**

Most studies have focused on the influence of single miRNAs in regulating AMPAR distribution during scaling, however, they have been inadequate in providing a holistic view of the miRNA-



mediated control of synaptic scaling (Hou *et al*, 2015; Letellier *et al*, 2014; Rajman *et al*, 2017; Silva *et al*, 2019). We found that loss of MOV10 function, single-handedly accounted for the loss of sGluA1/A2, accompanied by commensurate decrease in mEPSC amplitude, thus effectively recapitulating the post-synaptic events during downscaling (Figure 6). How AMPARs are downregulated post chronic bicuculline treatment? Similar to previous observation (Shepherd *et al*, 2006), our study showed that bicuculline-induced hyperactivity enhances Arc protein, a key regulator of AMPAR removal from synapses. The enhancement of Arc expression and reduction of sAMPARs after loss of MOV10 demonstrates Arc translation to be a crucial intermediate between miRISC remodelling and synaptic downscaling. The expression of Arc has been shown to be regulated by a set of miRNAs (Wibrand *et al*, 2012), thus reinforcing our hypothesis that in context of chronic hyperactivity miRISC remodelling will take place prior to the Arc translation.

In contrast to chronic hyperactivity driven loss of MOV10, its polyubiquitination and subsequent localized degradation at active synapses has been shown to occur within minutes upon glutamate stimulation of hippocampal neurons in culture or during fear memory formation in amygdala (Banerjee *et al*, 2009; Jarome *et al*, 2011). These observations indicate that MOV10 degradation is a common player involved in both Hebbian and homeostatic forms of plasticity. Hebbian plasticity paradigms triggers homeostatic scaling in neurons as a compensatory mechanism (Vitureira & Goda, 2013); these two opposing forms of plasticity must involve a combination of overlapping and distinct molecular players. Our data demonstrates the requirement of a rapamycin-sensitive, MOV10 degradation-dependent Arc translation in homeostatic scaling that is distinct from the rapamycin-insensitive dendritic translation of Arc

occurring during Hebbian plasticity (Na *et al*, 2016). We speculate that homeostatic and Hebbian plasticity engages distinct signalling pathways that converge at miRISC remodelling. Though most homeostatic scaling studies including ours used hippocampal neurons in culture to investigate the mechanistic details, the use of this model leaves a lacuna to evaluate how input-specific gene expression control at selective synapses during Hebbian plasticity influences compensatory changes across all synaptic inputs to achieve network homeostasis. Therefore, physiological relevance of homeostatic scaling needs to be studied in association with Hebbian plasticity in order to delineate factors contributing to proteostasis involving cell intrinsic and extrinsic variables within a circuit. In this context, the study of synaptic scaling during sleep poses distinct advantages. Homeostatic downscaling is a key attribute observed in excitatory neurons during sleep, where, in order to aid the consolidation of contextual memory, synapses undergo pervasive remodelling by a protein kinase A-dependent dephosphorylation and removal of sAMPARs (Diering *et al*, 2017). Sleep promotes mTORC1-mediated Arc translation that is necessary for consolidation of ocular dominance plasticity in the cat visual cortex (Seibt *et al*, 2012). Therefore, impact of sleep in memory consolidation is an effective paradigm to analyse how proteostasis at the synapses drive the homeostatic scaling on a larger scale. The kinetics of miRISC-dependent proteome remodelling during sleep and its correlation with synaptic events may be explored further in order to understand the extent to which syncretic translation and degradation processes influence the temporal resolution of scaling during such physiological functions.

## Author Contributions

S.B and S.S designed the study. S.S., and B.S. performed all experiments. S.S., B.S., and S.B. analyzed the data. J.P.C. provided critical comments on electrophysiology experiments and manuscript. S.V.S.M gave comments on manuscript. S.S. and S.B wrote the manuscript.

## Acknowledgement:

We thank Addgene for lentiviral vectors, Ken Kosik for MOV10 shRNA constructs, microscope facility of Regional Centre for Biotechnology, India, Utsav Mukherjee for confocal imaging, Rohini Roy for analyzing efficacy of RNAi and Premkumar Palanisamy for maintenance of transgenic animals. This work is supported by Ramalingaswami Fellowship from the Department of Biotechnology, Government of India and National Brain Research Centre core fund to S.B.

Authors declare no conflict of interest

## References:

- Banerjee S, Neveu P & Kosik KS (2009) A Coordinated Local Translational Control Point at the Synapse Involving Relief from Silencing and MOV10 Degradation. *Neuron* **64**: 871–884
- Bingol B & Schuman EM (2006) Activity-dependent dynamics and sequestration of proteasomes in dendritic spines. *Nature* **441**: 1144–1148
- Burrone J & Murthy VN (2003) Synaptic gain control and homeostasis. *Curr. Opin. Neurobiol.* **13**: 560–567
- Cajigas IJ, Will T & Schuman EM (2010) Protein homeostasis and synaptic plasticity. *EMBO J.* **29**: 2746–2752
- Chowdhury S, Shepherd JD, Okuno H, Lyford G, Petralia RS, Plath N, Kuhl D, Huganir RL & Worley PF (2006) Arc/Arg3.1 Interacts with the Endocytic Machinery to Regulate AMPA Receptor Trafficking. *Neuron* **52**(3): 445-59.

- Davis GW (2006) Homeostatic control of neural activity: From Phenomenology to Molecular Design. *Annu. Rev. Neurosci.* **29**: 307–323
- Diering GH, Nirujogi RS, Roth RH, Worley PF, Pandey A & Huganir RL (2017) Homer1a drives homeostatic scaling-down of excitatory synapses during sleep. *Science* (80-. ). **355**: 511–515
- Dörrbaum AR, Alvarez-Castelao B, Nassim-Assir B, Langer JD, Schuman EM (2020) Proteome dynamics during homeostatic scaling in cultured neurons. *Elife* **9**: e52939.
- Ehlers MD (2003) Activity level controls postsynaptic composition and signaling via the ubiquitin-proteasome system. *Nat. Neurosci.* **6**: 231–242
- Fonseca R, Vabulas RM, Hartl FU, Bonhoeffer T & Nägerl UV (2006) A Balance of Protein Synthesis and Proteasome-Dependent Degradation Determines the Maintenance of LTP. *Neuron* **52**: 239–245
- Gainey MA, Hurvitz-Wolff JR, Lambo ME & Turrigiano GG (2009) Synaptic scaling requires the GluR2 subunit of the AMPA receptor. *J. Neurosci.* **29**: 6479–6489
- Goold CP & Nicoll RA (2010) Single-Cell Optogenetic Excitation Drives Homeostatic Synaptic Depression. *Neuron* **68**: 512–528
- Gregersen LH, Schueler M, Munschauer M, Mastrobuoni G, Chen W, Kempa S, Dieterich C & Landthaler M (2014) MOV10 Is a 5' to 3' RNA Helicase Contributing to UPF1 mRNA Target Degradation by Translocation along 3' UTRs. *Mol. Cell* **54**: 573–585
- Hanus C & Schuman EM (2013) Proteostasis in complex dendrites. *Nat. Rev. Neurosci.* **14**: 638–648
- Henry FE, McCartney AJ, Neely R, Perez AS, Carruthers CJL, Stuenkel EL, Inoki K & Sutton MA (2012) Retrograde changes in presynaptic function driven by dendritic mTORC1. *J. Neurosci.* **32**: 17128–17142
- Henry FE, Wang X, Serrano D, Perez AS, Carruthers CJL, Stuenkel EL & Sutton MA (2018) A unique homeostatic signaling pathway links synaptic inactivity to postsynaptic mTORC1. *J. Neurosci.* **38**: 2207–2225
- Hou Q, Ruan H, Gilbert J, Wang G, Ma Q, Yao WD & Man HY (2015) MicroRNA miR124 is required for the expression of homeostatic synaptic plasticity. *Nat. Commun.* **6**:10045
- Ibata K, Sun Q & Turrigiano GG (2008) Rapid Synaptic Scaling Induced by Changes in Postsynaptic Firing. *Neuron* **57**: 819–826

- Jakawich SK, Neely RM, Djakovic SN, Patrick GN & Sutton MA (2010) An essential postsynaptic role for the ubiquitin proteasome system in slow homeostatic synaptic plasticity in cultured hippocampal neurons. *Neuroscience* **171**: 1016–1031
- Jayaraj GG, Hipp MS & Ulrich Hartl F (2020) Functional modules of the proteostasis network. *Cold Spring Harb. Perspect. Biol.* **12(1)**: a033951
- Jarome TJ, Werner CT, Kwapis JL, Helmstetter FJ (2011) Activity dependent protein degradation is critical for the formation and stability of fear memory in the amygdala. *PLoS One* **6(9)**: e24349.
- Keck T, Toyozumi T, Chen L, Doiron B, Feldman DE, Fox K, Gerstner W, Haydon PG, Hübener M, Lee HK, Lisman JE, Rose T, Sengpiel F, Stellwagen D, Stryker MP, Turrigiano GG & van Rossum MC (2017) Integrating Hebbian and homeostatic plasticity: The current state of the field and future research directions. *Philos. Trans. R. Soc. B Biol. Sci.* **372**:
- Kenny PJ, Zhou H, Kim M, Skariah G, Khetani RS, Drnevich J, Arcila ML, Kosik KS & Ceman S (2014) MOV10 and FMRP Regulate AGO2 Association with MicroRNA Recognition Elements. *Cell Rep.* **9**: 1729–1741
- Klein ME, Castillo PE & Jordan BA (2015) Coordination between translation and degradation regulates inducibility of mGluR-LTD. *Cell Rep.* **10**: 1459–1466
- Krichevsky AM, King KS, Donahue CP, Khrapko K & Kosik KS (2003) A microRNA array reveals extensive regulation of microRNAs during brain development. *Rna* **9**: 1274–1281
- Letellier M, Elramah S, Mondin M, Soula A, Penn A, Choquet D, Landry M, Thoumine O & Favereaux A (2014) MiR-92a regulates expression of synaptic GluA1-containing AMPA receptors during homeostatic scaling. *Nat. Neurosci.* **17**: 1040–1042
- Lissin D V., Gomperts SN, Carroll RC, Christine CW, Kalman D, Kitamura M, Hardy S, Nicoll RA, Malenka RC & Von Zastrow M (1998) Activity differentially regulates the surface expression of synaptic AMPA and NMDA glutamate receptors. *Proc. Natl. Acad. Sci. U. S. A.* **95**: 7097–7102
- Ma XM & Blenis J (2009) Molecular mechanisms of mTOR-mediated translational control. *Nat. Rev. Mol. Cell Biol.* **10**: 307–318
- Na Y, Park S, Lee C, Kim DK, Park JM, Sockanathan S, Huganir RL & Worley PF (2016) Real-Time Imaging Reveals Properties of Glutamate-Induced Arc/Arg 3.1 Translation in Neuronal Dendrites. *Neuron*

- O'Brien RJ, Kamboj S, Ehlers MD, Rosen KR, Fischbach GD & Huganir RL (1998) Activity-dependent modulation of synaptic AMPA receptor accumulation. *Neuron* **21**: 1067–1078
- Ostroff LE, Fiala JC, Allwardt B & Harris KM (2002) Polyribosomes redistribute from dendritic shafts into spines with enlarged synapses during LTP in developing rat hippocampal slices. *Neuron* **35**: 535–545
- Paolantoni C, Ricciardi S, de Paolis V, Okenwa C, Catalanotto C, Ciotti MT, Cattaneo A, Cogoni C & Giorgi C (2018) Arc 3' UTR splicing leads to dual and antagonistic effects in fine-tuning arc expression upon BDNF signaling. *Front. Mol. Neurosci.* **11**:145.
- Pozo K & Goda Y (2010) Unraveling mechanisms of homeostatic synaptic plasticity. *Neuron* **66**: 337–351
- Rajman M, Metge F, Fiore R, Khudayberdiev S, Aksoy Akse A, Bicker S, Ruedell Reschke C, Raoof R, Brennan GP, Delanty N, Farrell MA, O'Brien DF, Bauer S, Norwood B, Veno MT, Krüger M, Braun T, Kjems J, Rosenow F, Henshall DC, et al (2017) A microRNA-129-5p/Rbfox crosstalk coordinates homeostatic downscaling of excitatory synapses. *EMBO J.* **36**: 1770–1787
- Sanz E, Yang L, Su T, Morris DR, McKnight GS & Amieux PS (2009) Cell-type-specific isolation of ribosome-associated mRNA from complex tissues. *Proc. Natl. Acad. Sci. U. S. A.* **106**: 13939–13944
- Schanzenbächer CT, Langer JD & Schuman EM (2018) Time- and polarity-dependent proteomic changes associated with homeostatic scaling at central synapses. *Elife* **7**: e33322.
- Schanzenbächer CT, Sambandan S, Langer JD & Schuman EM (2016) Nascent Proteome Remodeling following Homeostatic Scaling at Hippocampal Synapses. *Neuron* **92**: 358–371
- Schwamborn JC, Berezikov E & Knoblich JA (2009) The TRIM-NHL Protein TRIM32 Activates MicroRNAs and Prevents Self-Renewal in Mouse Neural Progenitors. *Cell* **136**: 913–925
- Seibt J, Dumoulin MC, Aton SJ, Coleman T, Watson A, Naidoo N & Frank MG (2012) Protein synthesis during sleep consolidates cortical plasticity in vivo. *Curr. Biol.* **22**(8):676-82
- Shalgi R, Hurt JA, Krykbaeva I, Taipale M, Lindquist S & Burge CB (2013) Widespread Regulation of Translation by Elongation Pausing in Heat Shock. *Mol. Cell* **49**: 439–452
- Shepherd JD, Rumbaugh G, Wu J, Chowdhury S, Plath N, Kuhl D, Huganir RL & Worley PF (2006) Arc/Arg3.1 Mediates Homeostatic Synaptic Scaling of AMPA Receptors. *Neuron*

- Shigeoka T, Jung H, Jung J, Turner-Bridger B, Ohk J, Lin JQ, Amieux PS & Holt CE (2016) Dynamic Axonal Translation in Developing and Mature Visual Circuits. *Cell* **166**: 181–192
- Silva MM, Rodrigues B, Fernandes J, Santos SD, Carreto L, Santos MAS, Pinheiro P & Carvalho AL (2019) MicroRNA-186-5p controls GluA2 surface expression and synaptic scaling in hippocampal neurons. *Proc. Natl. Acad. Sci. U. S. A.* **116**: 5727–5736
- Sutton MA, Ito HT, Cressy P, Kempf C, Woo JC & Schuman EM (2006) Miniature Neurotransmission Stabilizes Synaptic Function via Tonic Suppression of Local Dendritic Protein Synthesis. *Cell* **125**: 785–799
- Sutton MA, Taylor AM, Ito HT, Pham A & Schuman EM (2007) Postsynaptic Decoding of Neural Activity: eEF2 as a Biochemical Sensor Coupling Miniature Synaptic Transmission to Local Protein Synthesis. *Neuron* **55**: 648–661
- Tai HC, Besche H, Goldberg AL & Schuman EM (2010) Characterization of the brain 26S proteasome and its interacting proteins. *Front. Mol. Neurosci.* **3**:12.
- Tatavarty V, Sun Q & Turrigiano GG (2013) How to scale down postsynaptic strength. *J. Neurosci.* **33**: 13179–13189
- Thiagarajan TC, Lindskog M & Tsien RW (2005) Adaptation to synaptic inactivity in hippocampal neurons. *Neuron* **47**: 725–737
- Turrigiano GG (2017) The dialectic of hebb and homeostasis. *Philos. Trans. R. Soc. B Biol. Sci.* **372**: (1715)
- Turrigiano GG & Nelson SB (2004) Homeostatic plasticity in the developing nervous system. *Nat. Rev. Neurosci.* **5**: 97–107
- Vitureira N & Goda Y (2013) The interplay between hebbian and homeostatic synaptic plasticity. *J. Cell Biol.* **203**: 175–186
- Warkocki Z, Krawczyk PS, Adamska D, Bijata K, Garcia-Perez JL & Dziembowski A (2018) Uridylation by TUT4/7 Restricts Retrotransposition of Human LINE-1s. *Cell* **174**: 1537-1548.e29
- Wibrand K, Pai B, Siripornmongkolchai T, Bittins M, Berentsen B, Ofte ML, Weigel A, Skaftnesmo KO & Bramham CR (2012) MicroRNA regulation of the synaptic plasticity-related gene Arc. *PLoS One* **7**(7):e41688.
- Wierenga CJ, Walsh MF & Turrigiano GG (2006) Temporal regulation of the expression locus of homeostatic plasticity. *J. Neurophysiol.* **96**: 2127–2133



## **Supplementary Information**

### **Synchrony between translation and proteasome-dependent degradation drives homeostatic scaling in excitatory synapses.**

Balakumar Srinivasan<sup>1#</sup>, Sarbani Samaddar<sup>1#</sup>, Sivaram V.S. Mylavarapu<sup>2</sup>, James P. Clement<sup>3</sup> and Sourav Banerjee<sup>1§</sup>

1. National Brain Research Centre, NH-8. Nainwal Mode, Manesar-122052, Haryana, India

2. Regional Centre for Biotechnology, NCR-Biotech Science Cluster, Faridabad-Gurgaon Expressway, Faridabad-121001, Haryana, India

3. Neuroscience Unit, Jawaharlal Nehru Centre for Advanced Scientific Research, Jakkur, Bengaluru-560064, Karnataka, India.

# These authors contributed equally to this work

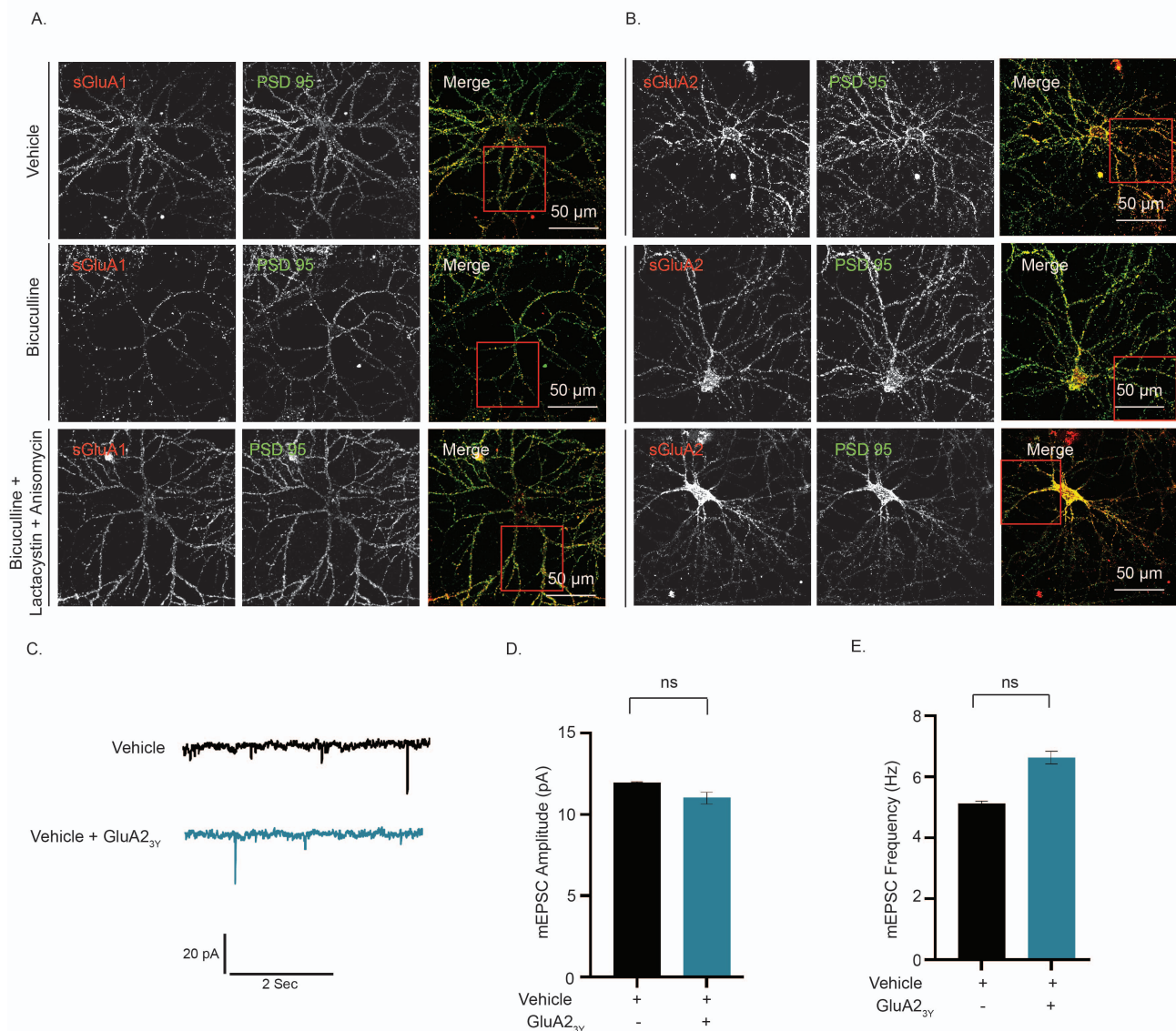
§ Correspondence

[souravnbrc@gmail.com](mailto:souravnbrc@gmail.com) OR [sourav@nbrc.ac.in](mailto:sourav@nbrc.ac.in) (S.B)



## Supplementary Figure

Figure: S1



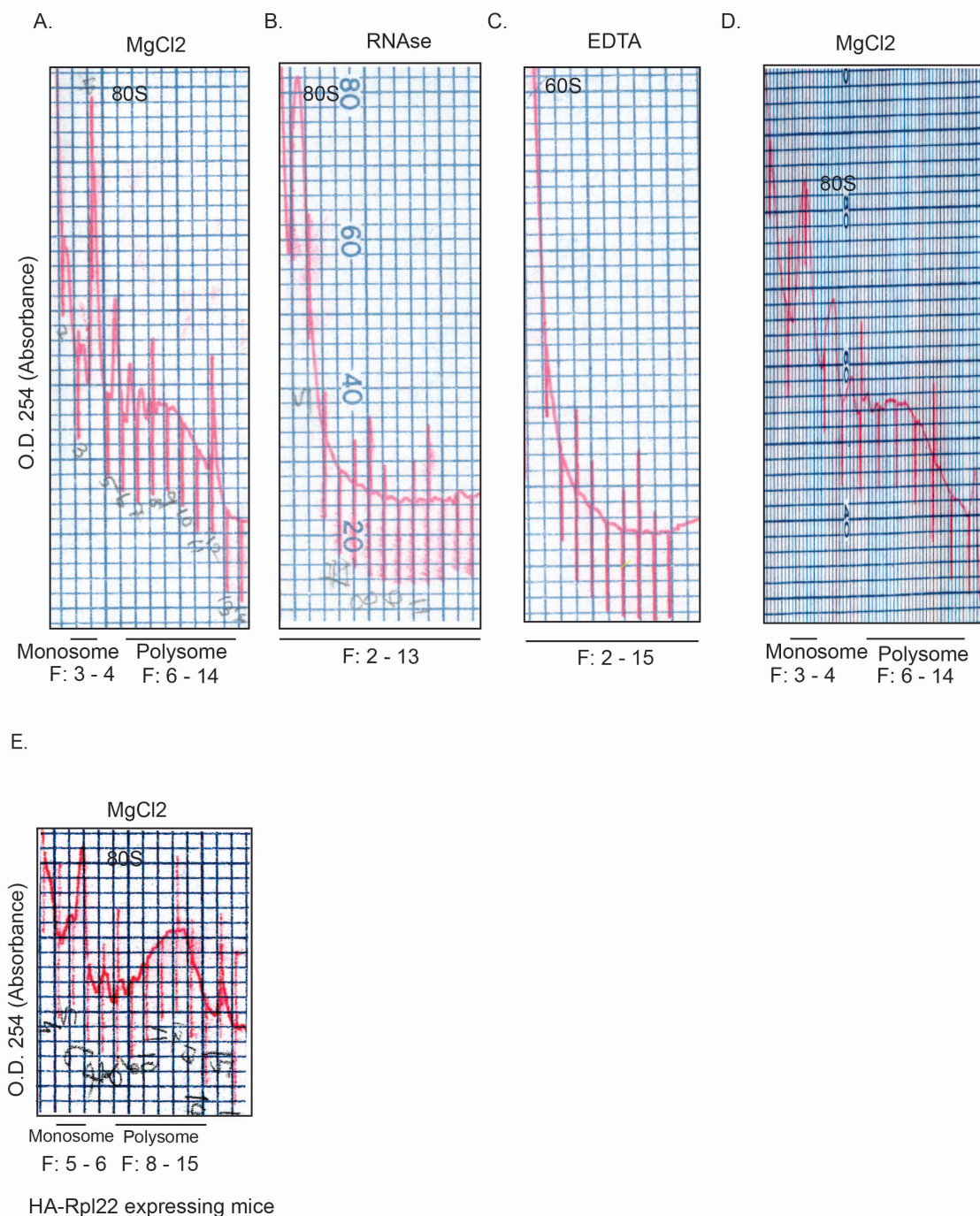
### Supplementary Figure 1: Synaptic downscaling by coordinated control of protein synthesis and degradation involves AMPARs.

(A-B) Hippocampal neurons were immunostained with GluA1 (A) or GluA2 (B) and PSD95 as described in Figure 2A-B. Photomicrograph showing images for surface GluA1 or GluA2 (red) and PSD95 (green) and sGluA1/PSD95 or sGluA2/PSD95 (merged). High magnification images of dendrites shown in Figure 2 marked in red square. Scale bar as indicated. Quantitation shown in Figure 2C-D.

(C-E) mEPSCs traces from hippocampal neurons (DIV18-24) treated with vehicle or GluA23y for 24 hours (C) as described in Figure 2E. Scale as indicated. Mean mEPSC amplitudes (D) and

frequencies (E) in neurons treated as indicated. n=12. Data shown as Mean  $\pm$  SEM. One Way ANOVA and Fisher's LSD.

Figure: S2

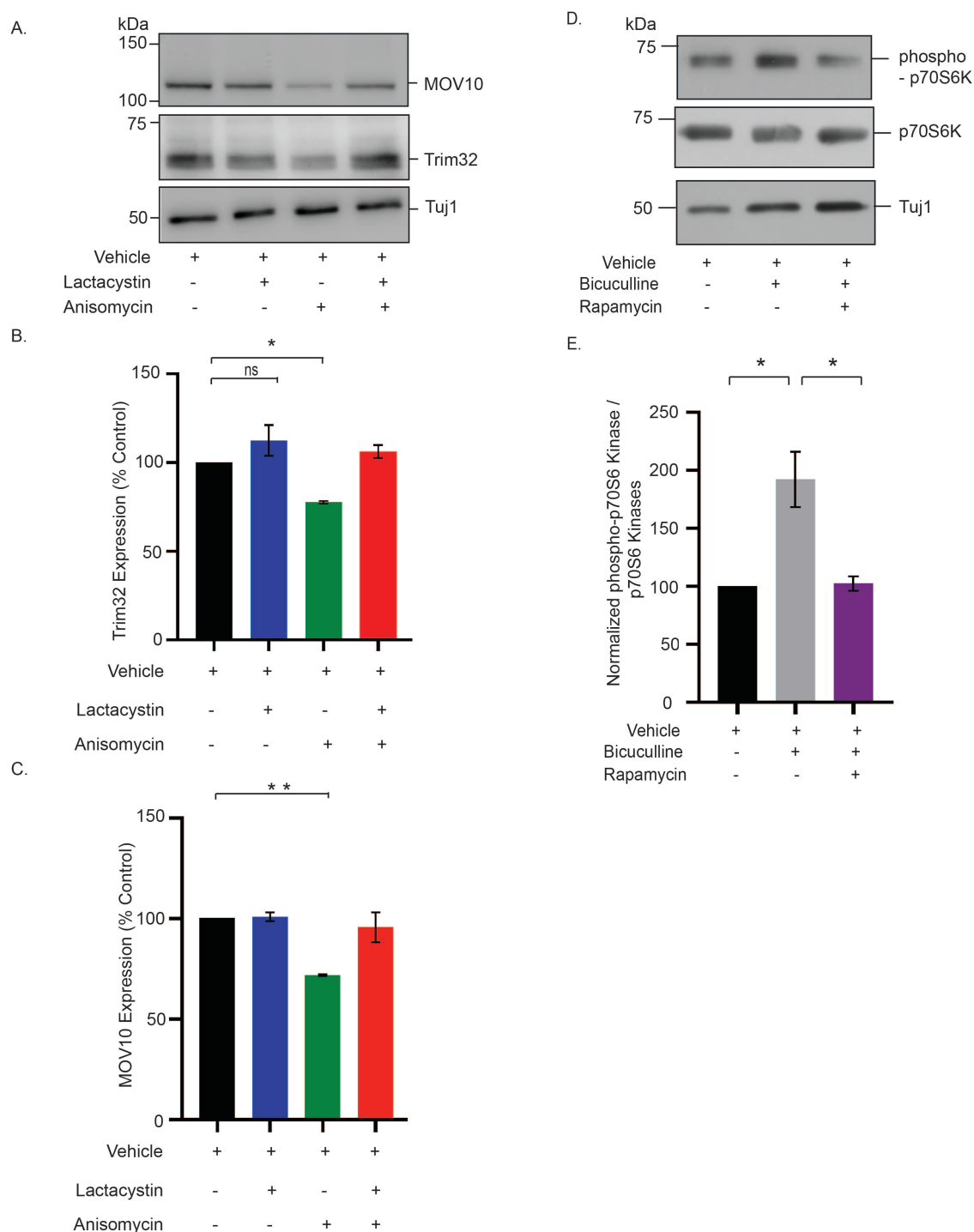


### Supplementary Figure 2: O. D<sub>254</sub> profile of polysome fractionation

(A-E) A<sub>254</sub> profile obtained from spectrophotometer attached gradient fractionator shown in Figure 3 and 4. Traces were drawn from original A<sub>254</sub> profile obtained from cytoplasmic extract treated with

MgCl<sub>2</sub> (A), RNase (B), EDTA (C), MgCl<sub>2</sub> (D) shown in Figure 3 and MgCl<sub>2</sub> treated extract from mouse expressing HA-Rpl22 in excitatory neurons (E) shown in Figure 4.

Figure: S3:



### Supplementary Figure 3: Expression profile of miRISC members and translation regulators under basal and activity-dependent conditions

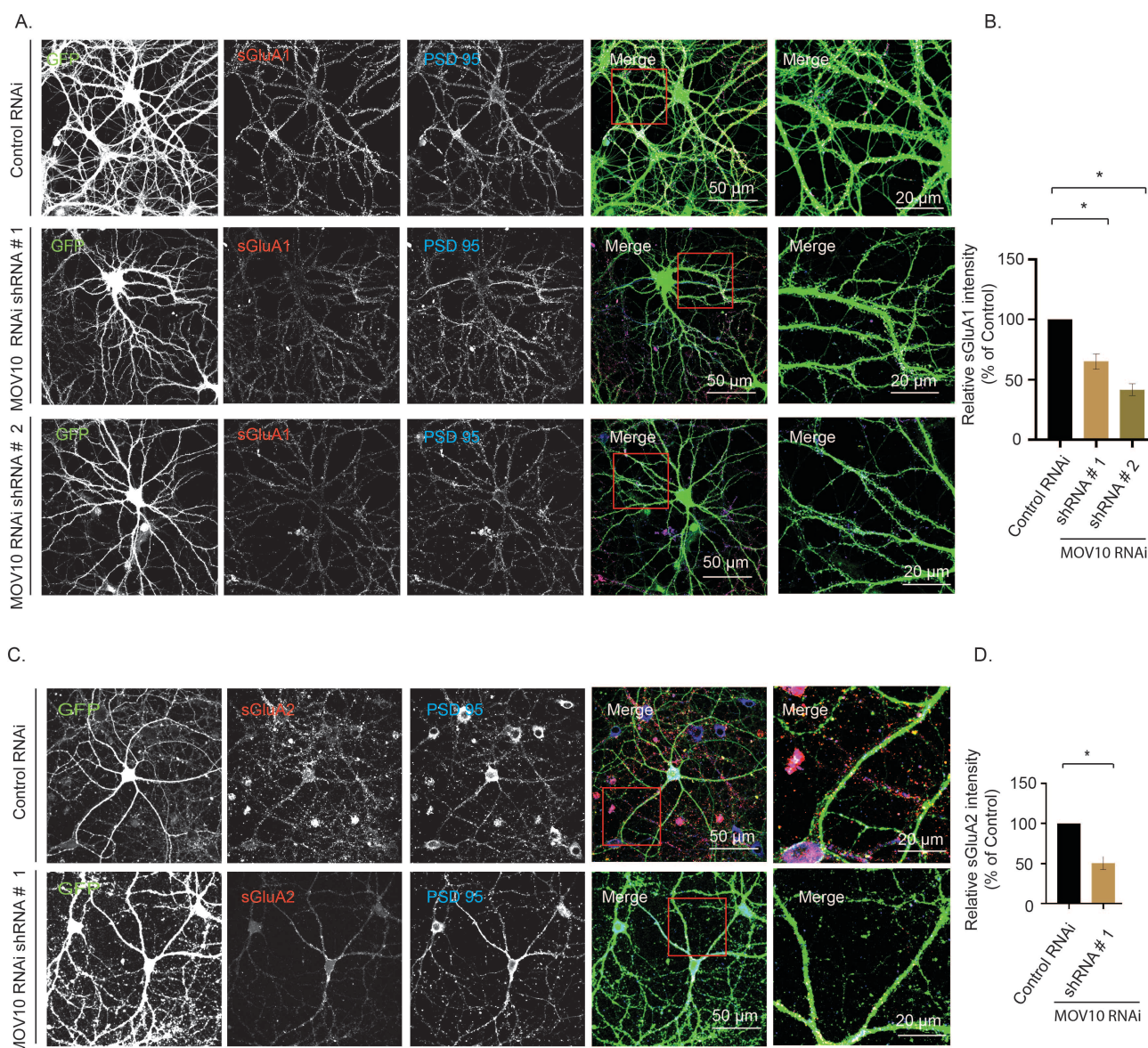
(A-C) Hippocampal neurons (DIV21) treated with lactacystin, anisomycin and both for 24 hours. Photomicrograph showing the expression of Trim32 and MOV10 as detected by



western blot analysis (A). Quantitation of Trim32 (B) and MOV10 (C). Data shown as Mean  $\pm$  SEM,  $n=3$ ,  $*p<0.001$  and  $**p<0.0003$ . One Way ANOVA and Fisher's LSD. See also Figure 5.

(D-E) Photomicrograph showing bicuculline treatment of hippocampal neurons (DIV21-22) enhanced phosphorylation of p70S6 Kinase (D). Quantitation of p70 S6 Kinase phosphorylation (E).  $n=4$ . Data shown as Mean  $\pm$  SEM,  $*p<0.001$ . One Way ANOVA and Fisher's LSD. See also Figure 5.

Figure: S4



# **Supplementary Figure 4:**

## **Surface AMPARs expression following MOV10 knockdown**

(A-B) Hippocampal neurons (DIV14-15) transduced with lentiviruses expressing two shRNAs against MOV10 (#1 or # 2) along with GFP. Transduced neurons (DIV21-24) were immunostained for surface GluA1 and co-immunostained for PSD95. Photomicrograph showing confocal images of GFP (green), sGluA1 (red), PSD95 (blue) and GFP/sGluA1/PSD95 (merged) (A). High magnification images of dendrites shown in Figure 6 marked in red square. Relative intensity of surface GluA1 particles at the synapse (overlap with PSD95 particles onto GFP expressing dendrites) (B). Normalized intensity of surface GluA1 relative to control was plotted. Data shown as Mean  $\pm$  SEM. \* $p < 0.01$ . One Way ANOVA and Fisher's LSD.

(C-D) Hippocampal neurons (DIV14-15) transduced with lentivirus expressing shRNA against MOV10 (#1) along with GFP. Transduced neurons (DIV21-24) were immunostained for surface GluA2 and PSD95. Photomicrograph showing confocal images of GFP (green), sGluA2 (red), PSD95 (blue) and GFP/sGluA2/PSD95 (merged). High magnification images of dendrites shown in Figure 6 marked in red square. Scale as indicated. Relative intensity of surface GluA2 particles at the synapse (overlap with PSD95 particles onto GFP expressing dendrites). Normalized intensity of surface GluA2 relative to control was plotted. Data shown as Mean  $\pm$  SEM. \* $p < 0.01$ . One Way ANOVA and Fisher's LSD.

## Supplementary Methods

### Primary neuronal culture

Hippocampal neuronal cultures from rat (Sprague-Dawley) were prepared and maintained as described previously (Kaeck & Banker, 2006). Briefly, hippocampi from embryonic day 18 (E18) pups were dissected, treated with trypsin (0.25%), dissociated by trituration to make single cell suspension and plated onto poly-L-lysine (1mg/ml) coated glass coverslip (160 – 250 cells / mm<sup>2</sup>). 160 - 170 cells /mm<sup>2</sup> were used for electrophysiology and surface labeling experiments. 200 - 250 cells /mm<sup>2</sup> cells were used for all biochemical experiments. Neurons were maintained in Neurobasal medium (Gibco) containing B27 supplements (Gibco) at 5% CO<sub>2</sub> / 37°C up to 25 days prior to commencement of experiments. Animal experiments were performed with the approval of the Institutional Animal Ethics (IAEC) committee of National Brain Research Centre.

### Lentivirus production and transduction

Lentivirus preparations and transduction into hippocampal neuronal cultures were performed as described previously (Banerjee *et al*, 2009). Validated shRNA against Trim32 (TATACCTTGCCTGAAGATC) (Schwamborn *et al*, 2009) was cloned into MluI and ClaI sites of pLVTHM vector (Addgene) and verified by sequencing. pLVTHM vectors containing MOV10 shRNA cassettes (sh#1:TTATACAAGGAGTTGTAGGTG) or (sh#2: ACTTAGCTCTAGTTCATAACC) (Banerjee *et al*, 2009) and non-targetting control (ATCTCGCTTGGGCGAGAGTAAG) were used for lentivirus preparation. *E. coli* Stbl3 strain was used to propagate pLVTHM plasmid and DH5α was used to propagate psPAX2 packaging plasmid (Addgene) and pMD2.G envelop plasmid (Addgene). Purified plasmids were prepared by Endo Free Maxiprep kit (Qiagen). Lentiviruses were produced by co-

transfection of 20µg transfer vector (EGFP cassette under EF1α promoter and shRNA cassette against MOV10 or Trim32 or non-targeting control under H1 promoter in pLVTHM plasmid), 15µg psPAX2 and 6µg pMD2.G into HEK293T cells. The cells were grown in low glucose DMEM media (Gibco) with 10% Fetal Bovine Serum (Gibco) and maintained at 5% CO<sub>2</sub> / 37°C. HEK293T (2×10<sup>6</sup> cells) were transfected by calcium phosphate method. Following transfections media containing transfection mixture was replaced with fresh media after 8 hours. Culture supernatant containing lentivirus particles were collected 72 hours post-transfection and concentrated virus stock was prepared by ultracentrifugation. Viral titers were determined by infecting HEK293T cells followed by FACS analysis. Typically, titer of concentrated viral stock was 1-2 × 10<sup>7</sup> TU/ml.

To perform RNAi, hippocampal neurons at Days *In Vitro* (DIV) 14-15 were infected with lentivirus expressing shRNAs against MOV10, Trim32 and non-targeting control respectively. We have used two shRNAs against MOV10 for its effective knockdown (data not shown) and also a non-targeting shRNA to eliminate the possibility of an off-target effect. Viral infections were performed at MOI of 1 for 6 hours and following infection lentivirus containing media was replaced with fresh Neurobasal media with B27 supplements. Neurons were incubated up to DIV25 prior to surface labeling and biochemical experiments. Viral infected neurons were tracked by EGFP expression for electrophysiology and imaging experiments.

## **Surface labeling of GluA1/A2**

Surface expression of AMPAR subunits (GluA1 or GluA2) was analyzed by live-labeling of hippocampal neurons with primary antibodies against surface epitopes of GluA1 (Millipore) or GluA2 (Millipore). Neurons (DIV 21-24) were immunostained as described previously (Schwarz *et al*, 2010). Prior to immunostaining, neurons were treated with vehicle



(DMSO), bicuculline (10 $\mu$ M) alone or in combination with lactacystin (10 $\mu$ M) and anisomycin (40 $\mu$ M) for 24 hours and transduced with lentivirus for effective knockdown of MOV10 expression. Live neurons were incubated for 15 minutes at 5% CO<sub>2</sub> / 37°C with N-terminus specific mouse GluA1 (1:25) or mouse GluA2 (1:10) antibodies diluted in Neurobasal media containing B27 supplements. Following incubation, the cells were washed twice with phosphate buffered saline containing Mg<sup>2+</sup> and Ca<sup>2+</sup> (PBS-MC; 137mM NaCl, 2.7 mM KCl, 10 mM Na<sub>2</sub>HPO<sub>4</sub>, 2mM KH<sub>2</sub>PO<sub>4</sub>, 1 mM Mg<sub>2</sub>Cl<sub>2</sub> and 0.1 mM CaCl<sub>2</sub>). Cells were then fixed in PBS-MC containing 2% paraformaldehyde and 2% sucrose for 20 minutes at 37°C, washed three times in PBS-MC at room temperature and blocked with PBS-MC containing 2% BSA for 30 minutes at room temperature. Cells were incubated with Alexa-546 conjugated goat-anti-mouse secondary antibody (1:200, Invitrogen) at room temperature for 60 minutes in blocking solution. Cells were permeabilized with PBS-MC containing 0.1% Triton-X-100 at room temperature for 5 minutes. Cells were further incubated with blocking solution for 60 minutes and then with goat PSD95 antibody (1:200, Abcam) for 8 hours at 4°C. Cells were incubated with Alexa-633 or Alexa-488 conjugated donkey-anti-goat secondary antibody (1:200, Invitrogen) at room temperature for 60 minutes. Cells were washed three times with PBS-MC at room temperature and mounted on Vectashield mounting media with DAPI (Vector Laboratories).

## Confocal Imaging and Image Analysis

Hippocampal neurons were imaged using a Leica TCS SP8 point scanning confocal microscope with a Leica Plan Apochromat 63X NA = 1.4 oil immersion objective at 1024 × 1024 pixel resolution. High magnification images were captured using 2X optical zoom. We have obtained 4-6 optical sections with 0.5 $\mu$ M step size. GFP and Alexa 488 were excited by 488 nM Argon laser. Alexa 546 and Alexa 633 were excited by solid state and



Helium-Neon lasers respectively. GFP, Alexa 488 and Alexa 546 signals were detected by hybrid detectors and Alexa 633 was detected by PMT. All images (8 bit) were acquired with identical settings for laser power, detector gain and pinhole diameter for each experiment and between experiments.

High magnification images, captured from confocal microscopy, were analyzed to observe the intensity of GluA1/A2 expression colocalizing with PSD95 (and GFP for MOV10 RNAi experiments). Images from the different channels were stacked and projected at maximum intensity using ImageJ (NIH). These images were then analyzed using custom written Matlab (Mathworks) programs. First, PSD95 and GFP image signals were thresholded to identify the pixels expressing PSD95 and GFP. Then, the pixels of GluA1/A2, colocalizing with PSD-95 and/or GFP were filtered and the average global intensity of these colocalizing GluA1 pixels were collected, plotted and further analyzed for statistics.

#### **Polysome fractionation and TCA precipitation of polysome fractions:**

Polysomes from the hippocampi of 8-10 week old SD rats were analyzed following previous protocol (Stefani *et al*, 2004). Following decapitation, the brains were removed and placed in ice-cold HEPES HBSS (HHBSS: 1× Hank's basal salt solution, 2.5 mM HEPES-KOH pH 7.4, 35 mM glucose, and 4 mM NaHCO<sub>3</sub>) containing 100 µg/ml of cycloheximide. From this point on, all procedures were done at 4°C. Hippocampi were dissected, pooled and homogenised in homogenization buffer (10 mM HEPES-KOH pH 7.4, 150 mM KCl, 5 mM MgCl<sub>2</sub>, and 0.5 mM DTT) containing EDTA-free protease and RNase inhibitors (Roche). 1.2mL of homogenization buffer per four hippocampi were used. Tissues were homogenised manually with a Dounce homogeniser and the homogenate was spun at 2000 × g, 10 min at 4°C to discard nucleus. The supernatant (S1) was collected and NP-40 was added to a final concentration of 1% v/v. After 5 min of

incubation on ice, S1 was spun at 20,000 g for 10 min, the resultant supernatant (S2) was loaded onto a 20-50% w/w linear density gradient of sucrose (Sucrose buffer: 10 mM HEPES-KOH pH 7.4, 150 mM KCl, 5 mM MgCl<sub>2</sub>). In the indicated conditions, EDTA (30mM) or a combination of RnaseT1 (Ambion,1000U/mL) and RnaseA (Ambion,40U/mL), was added to S2 and incubated for 10mins at room temperature before loading it onto the gradient. The gradients were centrifuged at 40,000 g, 2 hr at 4°C in a Beckman Instruments (Fullerton, CA) SW 41 rotor. Fractions of 0.75 ml volume were collected with continuous monitoring at 254 nm using an ISCO UA-6 UV detector. For HA-Rpl22 transgenic mice, exact protocols as above were followed. Hippocampi from 8-10 week old mice were homogenized and loaded onto the sucrose gradient. Tri-chloroacetic acid (TCA) was added to polysome fractions at 25% of their volume. All the fractions were incubated on ice for 30 mins post TCA addition followed by centrifugation at 13,000g for 30 mins at 4°C. The pellets were washed with ice-cold acetone (Merck) twice and dried. Acetone residues were allowed to evaporate and the pellets were resuspended in Laemmli buffer.

### **Proteasome activity assay**

Proteasome activity present in monosome and polysome fractions were analyzed by 20S Proteasome Assay Kit (Enzo Lifesciences) as per manufacturer's protocol. Briefly, 20S proteasome chymotrypsin-like activity was tested by incubating 80µl of each fraction with Suc-LLVY-AMC fluoregenic peptide substrate with or without epoxymycin (500nM) for 15 minutes at 30°C. Fluorescence was detected by fluoremeter (Tecan).

## Immunoprecipitation from HA-Rpl22 mice:

HA-tagged ribosomes from adult male mice were immunoprecipitated following previous protocol (Sanz *et al*, 2009) with minor modifications. RiboTag mice were crossed with CamKII-Cre mice and CamKII-Cre:RiboTag offspring expressing HA-epitope-tagged-Rpl22 were selected by genotyping. Prior to beginning the experiment, anti-HA-tagged beads (200µl) were washed twice with citrate-phosphate buffer pH-5, (24mM citric acid, 52mM dibasic sodium phosphate) and allowed to equilibrate twice for 5 minutes each in immunoprecipitation buffer (50mM Tris pH-7.5, 100mM KCl, 12mM MgCl<sub>2</sub>, 1% Nonidet P-40). Hippocampi from three adult (8-10 week old) HA-Rpl22 male mice were taken for preparing homogenates, along with the same number of age-matched RiboTag mice who do not express epitope-tagged Rpl22. Hippocampi were rapidly removed and weighed before homogenization in (10% w/vol) polysome buffer (50mM Tris pH-7.5, 100mM KCl, 12mM MgCl<sub>2</sub>, 1% Nonidet P-40(NP-40), 1mM DTT, 100µg/ml cycloheximide, EDTA free Roche Protease inhibitor cocktail, 200U/ml RNase Inhibitor) using a Dounce homogenizer. Homogenates were then pelleted at 5000g, 10 minutes at 4°C followed by collection of supernatant and re-centrifugation of the supernatant at 10,000g for 10 minutes at 4°C to create a post-mitochondrial supernatant. The supernatant was pre-cleared with protein-G agarose beads (Invitrogen) for 1 hour, followed by centrifugation at 8000g, 4°C, for 10 minutes to remove the beads. 2% of the total volume was kept aside as total input. The supernatant (250µl) was then incubated with the equilibrated anti-HA tagged affinity matrix for 6 hours with continuous mixing. The matrix was recovered by centrifugation at 8000g, 4°C for 15 minutes followed by two washes with high salt buffer HS-150 (Tris 50mM pH-7.5, KCl 150mM, MgCl<sub>2</sub> 12mM, 1% NP-40, DTT 1mM, 100µg/ml cycloheximide, protease and RNase inhibitors as above) for 5 minutes and two washes with high salt buffer HS-300 (Tris 50mM pH-7.5, KCl 300mM, MgCl<sub>2</sub> 12mM, 1% NP-40, DTT 1mM, 100µg/ml

cycloheximide, protease and RNase inhibitors as above) for 5 minutes. All procedures were done at 4°C. The pellets were boiled in Laemmli buffer and supernatant was used for Western Blot analysis.

## **Immunoprecipitation of 26S proteasome subunits and MOV10 from rodent hippocampus:**

Hippocampi of four adult (8-10 week old) male Sprague Dawley rats were collected and homogenized in tissue lysis buffer (50mM Tris pH-7.5, 150mM NaCl, 1% NP-40, 2mM EDTA, Roche protease inhibitor cocktail, 200U/ml Invitrogen RNase inhibitor, and phosphatase inhibitor cocktail (Sigma)) (10% w/vol) using a Dounce homogenizer. Prior to this, recombinant protein G-agarose beads (Invitrogen) were equilibrated in wash buffer WB-150 (10mM Tris pH8, 150mM NaCl, and 0.1% NP-40) twice for 5 mins each and centrifuged at 5000g for 2 minutes at 4°C to recover. The homogenates were centrifuged at 2000g, 4°C for 10 minutes followed by collection of supernatant and re-centrifugation at 10,000g at 4°C for 15 minutes to get a post-mitochondrial supernatant. Protein content of the supernatant was measured using the BCA protein estimation method (Pierce). 2% of the total protein content was kept aside as total input and the remaining was divided into two parts having equal protein content (~250µl each); one to be used for isotype control and the other for experiment purposes. Protein-G agarose beads were added (20µg) to each part and allowed to incubate with continuous mixing at 4°C for 1 hour. The pre-cleared supernatants were collected by centrifugation at 5000g for 10 minutes at 4°C. To the control fraction, 5µg of IgG isotype control was added (Mouse IgG in case of Rpt6 and Rabbit IgG in case of MOV10 immunoprecipitation). To the experimental fractions, 5µg of Rpt6 or MOV10 antibody was added and both fractions were allowed to incubate for 4 hours with continuous mixing. 40µg of proteinG agarose beads were added to the fractions

and further incubated for 2 hours. The beads were recovered by centrifugation and washed twice with wash buffer IPP-150 (50mM Tris pH7.5, 150mM NaCl, 12mM MgCl<sub>2</sub>, 1% NP-40 and 0.5 mM DTT along with RNase, protease and phosphatase inhibitors, see reagent list) followed by twice with IPP-300 (same constituents as IPP-150 except NaCl concentration is 300mM). In case of Rpt6, a further stringent wash with IPP-450 (450mM NaCl, rest same as IPP-150) was required. All procedures were done at 4°C. The total input, control and the immunoprecipitated samples were boiled in Laemmli buffer and stored for further analysis.

#### **Western Blot for immunoprecipitated samples and polysomes:**

Immunoprecipitated samples were analyzed as per previous protocols (Banerjee *et al*, 2009). Briefly, samples were boiled in Laemmli buffer and equal volumes resolved on a 8-10% SDS-PAGE. Post transfer of proteins on nitrocellulose membrane (Millipore), blots were blocked with 5% BSA for 1 hour and probed with primary antibodies overnight. In case of MOV10 IP samples, immunoblotting was done against itself (Bethyl Lab), Trim32 (Abcam) and Ago (Millipore). In case of Rpt6 IP samples, blots were probed for eEF2 (CST) p70S6 kinase (CST), phospho-P70S6 kinase and Rpt6 itself (Enzo) overnight at 4°C. See Reagent details for more information. Following extensive washing with Tris-Buffer-Saline containing 0.1% Tween-20 (0.1%TBST), secondary antibody supplied with the CleanBlot HRP detection kit (Thermo Scientific) was used to detect the proteins using standard chemiluminescence detection on X-ray films. Band intensities were quantified by densitometry using ImageJ software.

Equal volumes of TCA-precipitated polysome fractions were resolved on 8-10% SDS-PAGE and transferred onto PVDF membranes. Following blocking with 5% BSA, blots were probed with Rpt6, Rpt1, Rpt3 and 20Sα core subunit (Enzo), eIF4E and p70 S6

kinase (CST) overnight at 4°C. Post incubation, blots were washed with 0.1% TBST and probed with appropriate secondary antibodies. Blots were detected using standard chemiluminescence (Millipore ) detection.

### **Western Blot for primary neuron cultures:**

Cultured rat hippocampal neurons (DIV 21-24) were incubated with bicuculline (10μM), anisomycin (40μM), lactacystin (10μM), rapamycin (100nM) alone or in combination for 24 hours. Post incubation, cells were washed twice in pre-warmed phosphate buffer saline and collected in Laemmli buffer . Equal volumes of lysates were resolved on 8-10% SDS-PAGE, transferred onto nitrocellulose membrane, blocked with 5% BSA and probed with antibodies against MOV10 and Trim32. For each lane, immunoblotting was also performed with Tuj1 (Sigma) or as the internal control to normalize protein levels. Blots were detected using standard ECL chemiluminescence detection (Millipore) and band intensity determined by ImageJ. MOV10 and Trim32 RNAi samples were also detected similarly, but using GAPDH (Sigma) as the internal control.

### **Electrophysiology**

Whole cell patch clamp experiments were performed using primary hippocampal neurons (DIV18-25). Neurons were incubated with bicuculline (10μM), anisomycin (40μM), lactacystin (10μM), rapamycin (100nM) and GluA23y (10μM) for 24 hours. Neurons were patched with glass micro-electrodes with an open-tip resistance of 3-8MΩ. Cells with series resistance >30MΩ were excluded from the analysis. To measure the excitatory currents, the following composition of internal solution was used: 100mM Cesium gluconate, 0.2mM EGTA, 5mM MgCl<sub>2</sub>, 2mM ATP, 0.3mM GTP, 40mM HEPES, pH 7.2 (285-290 mOsm). Miniature EPSCs (mEPSCs) were recorded by holding the cells at -

70mV in a recording solution consisting of: 119mM NaCl, 5mM KCl, 2mM CaCl<sub>2</sub>, 2mM MgCl<sub>2</sub>, 30mM glucose, 10mM HEPES, pH7.4 (310-320 mOsm) in the presence of 1μM tetrodotoxin and 10μM Bicuculline.

Average of mEPSC events for 300s from each neuron was analyzed and only the events with <-4pA of peak amplitudes, >0.3pA/ms of rise rates, and 1-12ms of decay time constants were selected for the analysis.

All recorded signals were amplified by Multiclamp 700B (Molecular devices), filtered at 10 Khz and digitised at 10-50 KHz. Analog to digital conversion was performed using Digidata 1440A (Molecular Devices). All data were acquired and analysed using pClamp10.5 software (Molecular Devices) and custom Matlab filtering algorithms. Cells with holding currents greater than -100pA were excluded from the analysis, as well as any cell which was unstable during the recording.

### **Statistical Analysis:**

Statistical Analyses were performed for all experiments. Whole cell patch clamp amplitudes and frequencies were analyzed using one-way ANOVA with post-hoc Fisher's LSD test to test pairwise differences across the groups. Imaging and western blot data were analyzed for statistical significance using one-way ANOVA with post-hoc Fisher's LSD test. Western blot data related to RNAi experiment was analyzed using unpaired t-test with Welch's correction. Data is reported as absolute differences in mean ± SEM for electrophysiology data or percent differences in mean ± SEM for imaging and western blot data between groups.



## References:

- Banerjee S, Neveu P & Kosik KS (2009) A Coordinated Local Translational Control Point at the Synapse Involving Relief from Silencing and MOV10 Degradation. *Neuron* **64**: 871–884
- Kaech S & Banker G (2006) Culturing hippocampal neurons. *Nat. Protoc.* **1**: 2406–2415
- Sanz E, Yang L, Su T, Morris DR, McKnight GS & Amieux PS (2009) Cell-type-specific isolation of ribosome-associated mRNA from complex tissues. *Proc. Natl. Acad. Sci. U. S. A.* **106**: 13939–13944
- Schwamborn JC, Berezikov E & Knoblich JA (2009) The TRIM-NHL Protein TRIM32 Activates MicroRNAs and Prevents Self-Renewal in Mouse Neural Progenitors. *Cell* **136**: 913–925
- Schwarz LA, Hall BJ & Patrick GN (2010) Activity-dependent ubiquitination of GluA1 mediates a distinct AMPA receptor endocytosis and sorting pathway. *J. Neurosci.* **30**: 16718–16729
- Stefani G, Fraser CE, Darnell JC & Darnell RB (2004) Fragile X mental retardation protein is associated with translating polyribosomes in neuronal cells. *J. Neurosci.* **24**: 7272–7276